Simultaneous imaging and relative quantitation of multiple neurotransmitters in a progressive Parkinson's disease model by MALDI mass spectrometry

Elva Friðjónsdóttir

M. Sc. Thesis in Pharmacy

Supervisor: Margrét Þorsteinsdóttir

Faculty of Pharmaceutical Science

School of Health Science, University of Iceland

January 2016

Samtíma myndgreining og hlutfallsleg magngreining á taugaboðefnum í framsæknu Parkinsons-líkani með MALDI massagreiningu

Elva Friðjónsdóttir

Meistararitgerð í lyfjafræði

Umsjónarkennari: Margrét Þorsteinsdóttir

Lyfjafræðideild

Heilbrigðisvísindasvið Háskóla Íslands

Janúar 2016

Printing: Háskólaprent ehf.

Reykjavík, Iceland 2016

Author Elva Friðjónsdóttir

Supervisor Margrét Þorsteinsdóttir
Associate Professor
Faculty of Pharmaceutical Science,
Universtiy of Iceland

Instructors Per Andrén
Associate Professor
Biomolecular Imaging and Proteomics
Department of Pharmaceutical Bioscience,
Uppsala University

Anna Nilson
Senior Researcher
Biomolecular Imaging and Proteomics
Department of Pharmaceutical Bioscience,
Uppsala University

Mohammadreza Shariatgorji
Senior Researcher
Biomolecular Imaging and Proteomics
Department of Pharmaceutical Bioscience,
Uppsala University

The project was carried out at the research facilities of Biomolecular Imaging and Proteomics, Department of Pharmaceutical Bioscience,
Uppsala University.

ABSTRACT

Simultaneous imaging and relative quantitation of multiple neurotransmitters in a progressive Parkinson's disease model by MALDI mass spectrometry

Background: Parkinson's disease is a progressive degenerative disease that has an unknown pathogenesis. Research on Parkinson's disease models have provided valuable information contributing to the understanding of the disease. Recently developed methods allow imaging of multiple neurotransmitters by matrix assisted laser desorption/ionization – mass spectrometry imaging (MALDI-MSI). Applying MALDI-MSI to a Parkinson's disease model might reveal new information on neurotransmitter concentrations and distribution.

Objectives: MALDI-MSI was used to simultaneously image multiple neurotransmitters and metabolites in brain tissue sections of a progressive Parkinson's disease mouse model, with and without treatment with the dopamine agonist apomorphine. The MALDI-MSI results were used to perform relative quantification of neurotransmitters and their metabolites in selected regions in the brain to identify discripancies between the Parkinson's disease model and a healty control.

Methods: Brain tissue sections from a progressive Parkinson's disease mouse model, a Nurr1-knock-out (KO) model were used in this experiment. The tissue sections were prepared using recently developed methods for detecting multiple neurotransmitters. These methods include using two different derivatizing agents and two different MALDI matrixes. An in-house developed software was used to extract quantitative information of the neurotransmitters.

Results: The distribution of dopamine, 3-MT, GABA, serotonin, 5-HIAA, acetylcholine, α-GPC, glutamine, aspartate and glutamate was imaged. The relative quantification revealed that dopamine levels were reduced about 70% in the Nurr1 KO model, while acetylcholine was increased about 24%. Also glutamate, glutamine and aspartate seemed to be altered in the Nurr1 KO model.

Conclusions: Investigation of the concentrations of neurotransmitters in a progressive Parkinson's disease mouse model showed that not only dopamine levels were altered in the Parkinson's disease model, but also others neurotransmitters such as acetylcholine, glutamate, glutamine and aspartate. The present results give valuable information leading to deeper understanding of neurotransmission in early stages of Parkinson's disease.

ÁGRIP

Samtíma myndgreining og hlutfallsleg magngreining á taugaboðefnum í framsæknu Parkinsons-líkani með MALDI massagreiningu

Bakgrunnur: Parkinsonsveiki er taugahrörnunarsjúkdómur með óþekkta meingerð. Rannsóknir á Parkinsons-líkönum hafa veitt mikilvægar upplýsingar og aukið skilning á sjúkdómnum. Nýlegar aðferðir gefa þann möguleika að nota matrix assisted laser desorption/ionization mass spectrometry imaging (MALDI-MSI) til að myndgreina margvísleg taugaboðefni í vefjasneiðum. Ef þessum aðferðum er beitt á vefjasýni úr Parkinsons-líkani er mögulega hægt að fá nýjar upplýsingar um dreifingu og styrk taugaboðefna í Parkinsons-veiki.

Markmið: Nota MALDI-MSI til að myndgreina fjölda taugaboðefna og umbrotsefni þeirra í Parkinsons-líkani. Nota niðurstöðurnar til að gera hlutfallslega magngreiningu á taugaboðefnum í völdum svæðum í heilanum með því að bera saman við vef úr heilbrigðum músum. Einng að skoða hvort að dópamín örvinn, apomorphine, hafi áhrif á magn taugaboðefna.

Aðferðir: Heilasneiðar úr framsæknu Parkinsons-líkani, Nurr1 knock-out (KO) músa líkani, voru notaðar í þessari tilraun. Sneiðarnar voru meðhöndlaðar með nýlega þróuðum aðferðum sem fela í sér tvær mismunandi afleiðumyndanir og tvö mismunandi MALDI matrix. Sérstakur hugbúnaður, þróaður á rannsóknarstofunni, var notaður til fá magngreinandi upplýsingar um taugaboðefnin.

Niðurstöður: Dreifing á dópamíni, 3-MT, GABA, serótóníni, 5-HIAA, asetýlkólíni, α-GPC, glútamíni, aspartati og glútamati var myndgreind. Hlutfallsleg magngreining leiddi í ljós u.þ.b. 70% lækkun á dópamíni í Nurr1 KO líkaninu og u.þ.b. 24% hækkun á asetýlkólíni. Einnig virðist magn af glútamati, glútamíni og aspartati hafa breyst í líkaninu.

Ályktanir: Rannsókn á styrk taugaboðefna í framsæknu Parkinsons-líkani leiddi í ljós að það er ekki einungis dópamín styrkur sem breytist í Parkinsons-líkaninu heldur einnig önnur taugaboðefni. Þar má nefna asetýlkólín, glútamat, glútamín og aspartat. Niðurstöður þessarar rannsóknar gefa verðmætar upplýsingar sem dýpka skilning á taugaboðskiptum á fyrstu stigum Parkinsonsveiki.

ABBREVIATIONS

5-HIAA	5-hydroxyindoleacetic acid
6-OHDA	6-hydroxydopamine
9-AA	9-Aminoacridine
AADC	Aromatic L-amino acid decarboxylase
ACh	Acetylcholine
ANTH-MP	4-(anthracen-9-yl)-1-methylpyridinium
APO	Apomorphine
BG	Basal ganglia
CER	Cerebellum
CHCA	α-cyano-4-hydroxycinnamic acid
CP	Caudate Putamen
CTX	Cortex
DA	Dopamine
DAT	Dopamine transporter
DCHCA	d-α-cyano-4-hydroxycinnamic acid
dCP	dorsal Caudate Putamen
DL	Dorsal Lateral
DM	Dorsal Medial
DPP	2,4-diphenyl-pyranylium
GABA	γ-aminobutyric acid
Glu	Glutamate
GP	Globus Pallidus
GPe	Globus Pallidus externa
GPi	Globus Pallidus interna
H&E	Hematoxylin and eosin
HIP	Hippocampus
ITO	Indium tin oxide
KO	Knock-out
L-DOPA	L-3,4-dihydroxyphenylalanine
m/z	Mass-to-charge ratio
MALDI	Matrix assisted laser desorption/ionization
MPTP	1-methyl-4-phenyl-1,2,3,6-tetrahydropyridine

MSDB	Medial septum-diagonal band
MSI	Mass spectrometry imaging
NAc	Nucleus Accumbens
NE	Norepinephrine
NT	Neurotransmitter
OT	Olfactory tubercle
PCX	Prefrontal cortex
PD	Parkinson’s disease
RET	Ret receptor tyrosine kinase
ROI	Region of interest
SAL	Saline
SCX	Sensorimotor cortex
SD	Standard deviation
SEM	Standard error of the mean
SN	Substantia nigra
SNpc	Substantia nigra pars compacta
SNpr	Substantia nigra pars reticularis
STN	Subthalmic nucleus
TF	Transcription factor
TH	Tyrosine hydroxylase
TIC	Total ion count
TOF	Time-of flight
vCP	ventral Caudate Putamen
VIP	vasoactive intestinal peptide
VL	Ventral Lateral
VM	Ventral Medial
VMAT	Vesicular monoamine transporter
VTA	Ventral tegmental area
WT	Wild type

TABLE OF CONTENT

LIST OF TABLES

LIST OF FIGURES

1. INTRODUCTION

Parkinson's disease (PD) is a common neurodegenerative disease with a pathogenesis that remains largely unknown (de Lau & Breteler, 2006). Models for PD have been a very important tool in researching the disease both the older, more established toxin-induced models and the recent genetically engineered models (Dawson, Ko, & Dawson, 2010). The transcription factor (TF) Nurr1 has been linked to PD in several studies (Chu et al., 2006; Jankovic, Chen, & Le, 2005). Kadkhodaei et al. has established the importance of Nurr1 in maintenance of dopaminergic (DAergic) neurons and introduced the Nurr1 knock-out (KO) model as a slowly progressive PD model that mimics the early stages of the disease (Kadkhodaei et al., 2013). Recently published results from the biomolecular imaging and proteomics research group located in Uppsala, Sweden introduce methods that enable imaging of several neurotransmitters (NTs) using matrix-assisted laser desorption/ionization (MALDI) mass spectrometry (Shariatgorji et al., 2012, 2014). This research was performed in collaboration with a research group in the Department of Clinical Neuroscience in Karolinska Institutet, Stockholm, Sweden that had developed a genotype of Nurr1 KO mice in order to reseach PD (Kadkhodaei et al., 2013). The thesis focuses on examining the distribution and concentrations of NTs in brain tissue samples of this unique PD model by utilizing the newly developed MALDI-mass spectrometry imaging (MSI) neuroimaging methods.

1.1 Parkinson's disease

Parkinson's disease is a neurodegenerative disease that affects over 1% of the world population over 65 years of age. It is the second most common neurodegenerative disease after Alzheimer's disease. It is characterized by motor impairment such as resting tremors, postural impairment, bradykinesia and rigidity. Patients suffer also from non-motor symptoms such as depression, behavioral changes, autonomic dysfunction, fatigue and sleep disorders (Chaudhuri & Schapira, 2009; Pfeiffer, 2015).

The clinical symptoms of PD were first described by James Parkinson in 1817 when he referred to it as "the shaking palsy" (Jankovic, 2008). Over a hundred years later it was discovered that patients lost neurons in the substantia nigra (SN). In 1960 researchers found out that dopamine (DA) concentrations was remarkably reduced in the striatum of patients (Ehringer & Hornykiewicz, 1960). This led to the trial of L-DOPA treatment in PD patients and showed significant improvement in bradykinesia (Jankovic, 2008). Since then researchers

have focused on finding the cause of the degeneration of the DAergic neurons. Many factors seem to contribute to the pathology of the disease and it is hypothesized that it is caused by complex interactions between environmental and genetic factors (Gubellini & Kachidian, 2015).

1.1.1 Symptoms and diagnosis of Parkinson's disease

The onset of symptoms is gradual and may be misinterpreted or unnoticed for a long time before diagnosis. It starts with impairment of dexterity or a slight dragging of one foot and then fatigue, stiffness and extreme slowing down (Lees, Hardy, & Revesz, 2009).

Slowness of movement, referred to as bradykinesia or akinesia, is the most characteristic clinical feature of PD. The most common and easily detectable symptom is tremor at rest that disappears during movement. (Jankovic, 2008). Patients develop rigidity or stiff limbs because muscles are not able to relax normally (Berardelli, Sabra, & Hallett, 1983). The last typical motor symptom is postural abnormalities that occurs in the late stages of PD. When this happens control of orientation and stabilization is lost. This can be dangerous to patients because of increased risk of falls and injuries caused by loss of autonomic reflexes (Benatru, Vaugoyeau, & Azulay, 2008).

Non-motor symptoms are also important and can highly affect the quality of life. Depression, anxiety, sleep disorders, constipation and pain are only a few symptoms that might develop. Majority of patient experiences one or more types of non-motor symptoms. Some of these symptoms may appear before motor impairment and they become severe when the disease progresses (Chaudhuri, Healy, & Schapira, 2006; Pfeiffer, 2015).

The diagnosis of PD is based on evaluating clinical features. The disease has a long pre-symptomatic phase and when symptoms appear 50-70% of DA neurons are already lost and striatal DA level have declined about 70-80% (Jankovic, 2008; Mollenhauer & Zhang, 2012; Müller, 2012; Terzioglu & Galter, 2008). A recent study reported that accuracy of clinical diagnosis is about 80% and hasn't improved in recent years (Rizzo et al., 2015). Also non-motor symptoms are often poorly recognized and remain undiagnosed for a long time (Chaudhuri et al., 2006). The search for new biomarkers is ongoing. The identification of a novel biomarker could help the diagnosis and provide endpoints to evaluate clinical efficiency, for example in neuroprotective therapy (Michell, Lewis, Foltynie, & Barker, 2004).

1.1.2 Treatment of Parkinson's disease

Current treatments for Parkinson's disease are limited to give only symptomatic relief but do not stop or slow down the progression of the disease. A better understanding of the disease process is vital to develop neuroprotective treatment.

The biological precursor of DA, L-DOPA, is the golden standard treatment for PD (Kakkar & Dahiya, 2015). Most patients respond well to L-DOPA but in long term the majority develops dyskinesia. These are involuntary movements that can be very disabling for the patient (Bastide et al., 2015; Sharma, Singh, Sharma, Singh, & Deshmukh, 2015). Dopamine agonists are also used to treat PD. They can be used along with L-DOPA or as monotherapy. There are evidence that use of DA agonists delay the onset of L-DOPA induced dyskinesia (Bonuccelli, Del Dotto, & Rascol, 2009; Hisahara, Shimohama, Hisahara, & Shimohama, 2011).

1.1.3 Genetics

The majority of Parkinson's disease cases are sporadic but about 10% are familial (de Lau & Breteler, 2006). Increasing number of genes and proteins are being linked to the disease. At least 5 distinct genes have been linked to sporadic PD. They are α-synuclein gene, parkin, DJ-1 PINK1 and LRRK2 (Gasser, 2001). Mutations or polymorphisms in these genes can be a contribution factor to development of PD. (Gasser, 2001; Gautier, Corti, & Brice, 2014; Hardy, Lewis, Revesz, Lees, & Paisan-Ruiz, 2009; Zheng, Heydari, & Simon, 2003, p. 1).

1.2 Pathology of Parkinson's disease

The pathology of Parkinson's disease is characterized by loss of DAergic neurons in the substantia nigra pars compacta (SNpc) that leads to reduced levels of DA in the midbrain and dysfunction of the basal ganglia (BG) (Gautier et al., 2014). Another hallmark is the presence of protein aggregates called Lewy bodies (LBs) that accumulate in patients brains (Santos & Cardoso, 2012). The main substance of the LBs is the protein α-synuclein (Wakabayashi, Tanji, Mori, & Takahashi, 2007). The etiopahtogenesis of PD remains unknown but it has been linked to several different factors such as mitochondrial function and abnormal protein folding.

1.2.1 Mitochondrial dysfunction

Mitochondrial dysfunction and oxidative stress have been shown to play a major role in the neurodegeneration. Several evidence that link mitochondrial dysfunction to PD exists but it is

debatable if it is the original cause or an effect (Cardoso, 2011; Gautier et al., 2014; Santos & Cardoso, 2012; Schapira, 2008). Mitochondria is the power source of the cell, it creates ATP from several oxidation reactions via the mitochondrial respiratory chain. It also has a role in regulation of cell death and production of reactive oxygen species (Lin & Beal, 2006). The function of midbrain DA neurons is highly energy demanding and therefore there is a high requirement of ATP-generating phosphorylation. DA neurons in SNpc and the ventral tegmental area (VTA) contain higher levels of mitochondrial DNA than other brain regions, (Fuke, Kubota-Sakashita, Kasahara, Shigeyoshi, & Kato, 2011) which establishes that sufficient mitochondrial function is very important to these cells (Kadkhodaei et al., 2013).

1.2.2 Abnormal protein folding

Most proteins have to fold in a specific three-dimensional structure in order to function. Misfolding leads to protein aggregation and may generate toxic species. Abnormal protein folding and age related decline in proteostasis has been suggested as a cause of PD (Hartl, Bracher, & Hayer-Hartl, 2011). The dysfunction in protein folding and degradation systems are have been linked to the aggregation of α-synuclein (Breydo, Wu, & Uversky, 2012; Wakabayashi et al., 2007).

1.2.3 Neurotransmission in Parkinson's disease

Neurotransmitters deliver signals in neuronal communication. They are distributed widely in the central nervous system and changes in their concentration trigger neuronal processes such as sleep, pain and aging (Benson et al., 2015; Cantor, 2015; Segovia, Porras, Del Arco, & Mora, 2001; Shetty & Bates, 2015). Abnormal changes in NTs concentrations contribute to disease state such as Parkinson's disease, Alzheimer's disease, depression and schizophrenia. The basal ganglia (BG) is crucial in motor and cognitive function (Brown & Marsden, 1998). DAergic dysfunction triggers a cascade that affects the whole BG network (Blandini, Nappi, Tassorelli, & Martignoni, 2000; Weingarten, Sundman, Hickey, & Chen, 2015).

1.2.3.1 The basal ganglia

The basal ganglia is comprised of several nuclei, the striatum, the substantia nigra (SN), globus pallidus (GP) and the subthalmic nucleus (STN). These structures are interconnected and communicate to control motor movement. The communication occurs mainly with inhibitory and excitatory input mediated via the neurotransmitters (NTs) GABA and

Glutamate (Glu) respectively (Weingarten et al., 2015). DA also plays a significant role in the BG communication with activation of D1 and D2 receptors in the dorsal striatum (Weingarten et al., 2015).

The basal ganglia receives excitatory input in the caudate putamen (CP), the dorsal part of striatum, from the cerebral cortex. Output from basal ganglia is inhibitory, GABAergic, from globus pallidus interna (GPi) and substantia nigra pars reticularis (SNpr) to the thalamus. There are two pathways between the CP and the GPi, the direct and indirect. The direct pathway originates in the CP and projects to the GPi and is GABAergic. The indirect pathway is polysynaptic and begins in the CP and goes to the globus pallidus externa (GPe) to the STN and then to the GPi. Input in both of these pathways lead to decreased inhibitory output from GPi to the thalamus which results in increased activity of the motor regions of the cortex (Weingarten et al., 2015). Figure 1 shows a simplified scheme of these pathways.

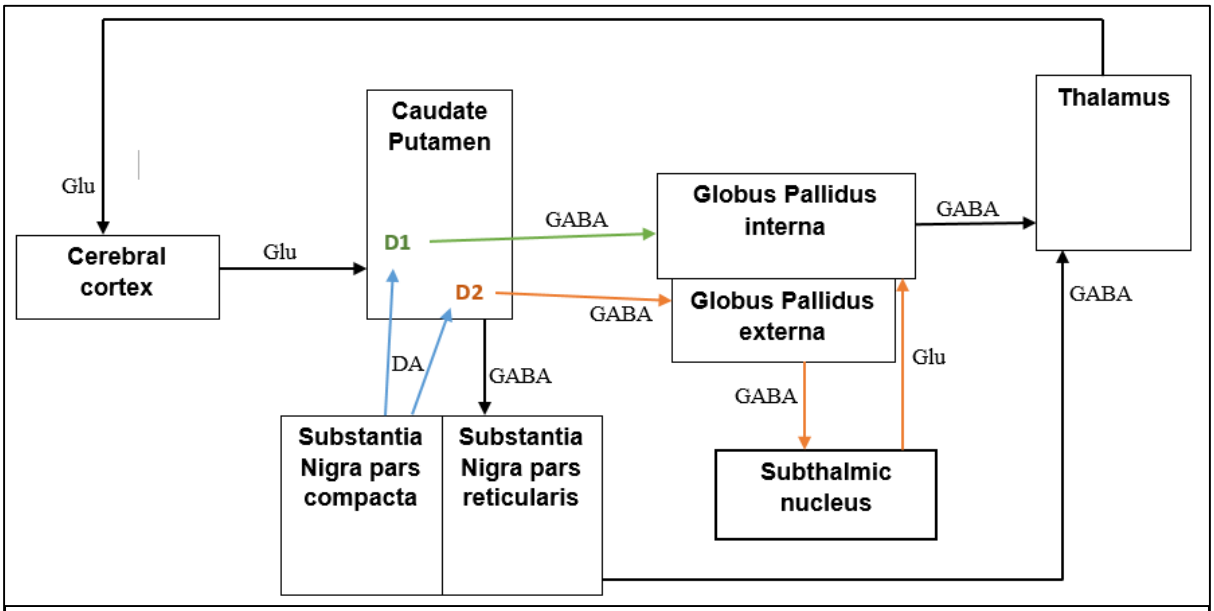

Figure 1. A simplified scheme of the cortico – basal ganglia – thalmocortical motor circuit. The green arrow indicates the direct pathway. Orange arrows indicate the indirect pathways. Blue arrows indicate the DAergic nigrostiatal pathway. DA binds to either D1 receptor or D2 receptors and activates the direct or indirect pathway

The nigrostriatal pathway originates from the SNpc and projects to the CP. The DAergic neurons with cell bodies in the SNpc project DA to the CP. The DA receptor D1 activates the direct pathway and D2 activates the indirect pathway (Weingarten et al., 2015). Ultimately DAergic output from SNpc promotes activation of the motor cortex. In contrast loss of DAergic output results in decreased motor activity (Weingarten et al., 2015).

1.2.3.2 Neurotransmitters affected in Parkinson's disease

There are six small neurotransmitters that are thought to be the most important in Parkinson's disease, i.e., dopamine, acetylcholine, GABA, glutamate, serotonin and norepinephrine (Weingarten et al., 2015).

1.2.3.2.1 Dopamine

The major dopamine (DA) synthesizing neurons project from in SNpc and VTA. DA is synthesized form the amino acid tyrosine. The first and rate limiting step of DA synthesis is a hydroxylation to form L-DOPA and is regulated by the enzyme tyrosine hydroxylase (TH). L-DOPA is then converted to DA via aromatic L-amino acid decarboxylase (AADC). After synthesis DA is stored in the cytoplasmic vesicles employing vesicular monoamine transporter (VMAT). DA is released from the vesicles into the synaptic cleft or extra synaptic space during neurotransmission. After neurotransmission there is either reuptake of DA back into the neurons via DA transporter (DAT) and stored in vesicles for reuse or DA is metabolized via catechol-O-methyltransferase or monoamine oxidase (Weingarten et al., 2015).

The striatum is divided into two parts, the dorsal part comprised of the CP and the ventral part comprised of the nucleus accumbens (NAc) and the olfactory tubercle (OT). SNpc projects DA to the dorsal part of the striatum whereas the VTA projects DA to the ventral part. This pathway is in the center of the reward circuit and the mesolimbic system (Weingarten et al., 2015). The dorsolateral prefrontal cortex is a key region in executive function and it is connected to the dorsal part of the caudate. The hippocampus (HIP) degenerates in late stages of PD and leads to memory impairment and other cognitive dysfunction (Weingarten et al., 2015).

1.2.3.2.2 Acetylcholine

Acetylcholine (ACh) is synthesized by neurons of the nucleus basalis of Meynert and septal nuclei. They innervate the cerebral cortex, amygdala, HIP and thalamus. The pedunculopontine nucleus projection neurons also synthesizes ACh and innervate SNpc, thalamus, hypothalamus and cerebellar nuclei. Also synthesized by striatal interneurons in CP and NAc. ACh is synthesized from choline and acetyl-CoA and is carried out in the cytoplasm via choline acetyltransferase. It is transferred into vesicles by vesicle-associated transporter. During neurotransmission ACh is released into synaptic cleft where it binds to either muscarininc receptor or nicotinic receptor. ACh is deactivated by acetylcholine esterase in the synaptic cleft.

Balance between DA and ACh is an important factor in PD. When DA levels decline in PD a relative hyperactivity in cholinergic function versus DAergic function develops in the striatum (Calabresi, Picconi, Parnetti, & Di Filippo, 2006). This can increase motor dysfunction that can be improved by anticholinergic treatment (Kakkar & Dahiya, 2015).

1.2.3.2.3 γ-Aminobutyric acid and glutamate

Glutmatergic and GABAergic pathways play central roles in the cortico-basal ganglia-thalmocortical circuit (Figure 1). The excitatory Glutamate (Glu) is projected from the thalamus to the cerebral cortex and from the cerebral cortex to the CP. GABA and Glu both deliver signals between internal structures of the basal ganglia (BG). The main output from the BG is from the SNpr and GPi and is inhibitory GABAergic. Approximately 90% of the neurons in the striatum are projection neurons and they are all GABAergic (Weingarten et al., 2015).

1.2.3.2.4 Serotonin and norepinephrine

Serotonin is synthesized from tryptophan in the raphe nuclei of the medulla and pons. Serotonergic projection neurons project serotonin to several regions in the brain including; the substantia nigra, caudate putamen, globus pallidus, thalamus, hippocampus and nucleus accumbens (Weingarten et al., 2015). Noprepinephrine (NE) is synthesized from DA by the enzyme dopamine β-hydroxylase in the projection neurons of the locus coeruleus (Weingarten et al., 2015). In PD the locus coeruleus degenerates and output of NE is decreased (Goedert, Spillantini, Del Tredici, & Braak, 2013). Degeneration of serotonergic neurons begins relatively early in the progression of the disease (Goedert et al., 2013). The loss of serotonin and NE in PD has been central to many theories and treatments of affective disorders such as depression (Bomasang-Layno, Fadlon, Murray, & Himelhoch, 2015; Eskow Jaunarajs, Angoa-Perez, Kuhn, & Bishop, 2011).

1.3 Experimental models of Parkinson's disease

Animal models have proven to be very important in researching Parkinson's disease. They have led to important discoveries about the pathogenesis of PD and to development of symptomatic treatment (Duty & Jenner, 2011). These studies have led to the hypothesis that the cause of the disease is due to a complex interaction between genetic and environmental factors (Gubellini & Kachidian, 2015). Since current treatments are only symptomatic, but not neuroprotective, establishment of new drug targets are needed. A deeper understanding of the early stages of PD is crucial for identification of such targets. Animal models that slowly

progress PD and mimic the early stages are a very useful tool to use in this purpose (Duty & Jenner, 2011).

1.3.1 Toxin induced models

The simplest and most commonly used models in research are neurotoxin induced models. They are well established and good models to simulate the features of late stage PD. These models are based on induction of oxidative stress that selectively damage the DAergic neurons. The 6-hydroxydopamine (6-OHDA) lesioned rodent and the 1-methyl-4-phenyl-1,2,3,6-tetrahydropyridine (MPTP) lesioned primate are the most used toxin induced PD models (Dawson et al., 2010). However, it is important to mention that the acute ablation of DA nerves in these models do not provide the opportunity to research the early stages of the disease.

1.3.2 Genetically engineered models

Since Parkinson's disease (PD) is a slowly progressive disorder a model that mimics the slowly degenerative nature of the disease is needed. Recent models have been designed based on genes associated with familial PD as well as genes that have been associated with sporadic PD (Dawson et al., 2010). Mutations in these genes have given insight into molecular mechanisms of PD. Some of them have exhibited mitochondrial dysfunction and abnormal protein folding, the same mechanisms of neuronal death as in sporadic PD (Duty & Jenner, 2011). Most of these modifications did not recapitulate the nigrostriatal neuronal degeneration, but led to a variety of abnormalities in the brain and spinal cord (Duty & Jenner, 2011). Dawson et. al. concluded in 2010 that none of the existing vertebrate models are particularly useful for investigating the selective vulnerability of the DA neurons (Dawson et al., 2010). A combinatorial study of all of the different genetically engineered models that have been developed should provide a better insight into PD pathogenesis.

1.4 A progressive model of Parkinson's disease – The Nurr1 knock-out model

1.4.1 The Nurr1 protein

The Nurr1 protein is a transcription factor (TF) that belongs to the nuclear receptor family. It binds to specific sequences in DNA and induces transcription of its target genes. It can bind either as a monomer, homodimer or a heterodimer with RXR. There is no known endogenous ligand for the Nurr1 receptor and it lacks a hydrophobic pocket which suggests that it might

function as a ligand-independent nuclear receptor (Decressac, Volakakis, Björklund, & Perlmann, 2013).

Already in 1997 the importance of Nurr1in DA neuron development was demonstrated in a study on Nurr1 KO mice. The *Nurr1*$^{-/-}$ KO mice failed to differentiate midbrain DA neurons, were hypoactive, not able to feed and died soon after birth (Zetterström et al., 1997). More recent studies have established the importance of Nurr1 in development and maintenance of DA neurons.

Several TFs with a key role in midbrain DAergic neuron development have been identified (Hegarty, Sullivan, & O'Keeffe, 2013; Simon, Bhatt, Gherbassi, Sgadó, & Alberí, 2003). Together these TFs control and induce the generation, differentiation and manifestation of the midbrain DA neurons (Hegarty et al., 2013; Simon et al., 2003). They work as a network and if any of them are missing in development it results in a severe defect in the midbrain DAergic system (Hegarty et al., 2013). In the later stages of development phenotypic expression starts and it is controlled by several TF including; Lmx1b, Nurr1, Engrailed-1, Engrailed-2 and Pitx3 (Hegarty et al., 2013). Lmx1b is essential for expression of Pitx3, a factor that seems to be critical to TH expression in SNpc DAergic neurons (Maxwell, Ho, Kuehner, Zhao, & Li, 2005). Following expression of Lmx1b, Nurr1 is expressed. Nurr1 regulates the development of the NT phenotype and participates in differentiation of midbrain DAergic progenitors into mature neurons. The Nurr1 protein allows these neurons to use DA as their NT by inducing expression of several proteins involved in DA synthesis and transport (Simon et al., 2003). These proteins include the TH, VMAT, AADC and DAT (Jankovic et al., 2005; Smidt & Burbach, 2007). It is interesting to note that the requirement of Nurr1 in phenotypic development in restricted to midbrain DAergic neurons alone and DA neurons outside the midbrain develop normally without Nurr1 (Simon et al., 2003).

The level of Nurr1 expression varies throughout different stages in life. It is highest in the embryonic stage but it maintains its expression in midbrain DA neurons throughout life (Jankovic et al., 2005; Zetterström et al., 1997). At least 95% of all TH positive midbrain neurons continue to express Nurr1 in adulthood (Bäckman, Perlmann, Wallén, Hoffer, & Morales, 1999).

The Ret receptor tyrosine kinase (RET) is a receptor for the glial cell line-derived neurotrophic factor (GDNF), a tropic factor that delivers survival and differentiation signal to the cell. RET is involved in maturation of DA neurons particularly for cell survival and fiber

innervation (Li et al., 2006). The expression of RET is induced by Nurr1 and RET expression has been shown to decrease in PD (Decressac et al., 2012; Galleguillos et al., 2010). Nurr1 also regulates expression of vasoactive intestinal peptide (VIP) (Luo, 2012). This peptide has shown to give neuroprotective effects in toxic condition (Delgado & Ganea, 2003). The reduced expression of RET and VIP via Nurr1 depletion should increase the vulnerability of the Nurr1 dependent DAergic neurons.

Nurr1 is involved in regulation of several nuclear mitochondrial genes. In a Nurr1 KO mouse model mitochondrial genes involved in oxidative respiration were reduced by 90% (Kadkhodaei et al., 2013). Since the cause of degeneration of neurons in PD is often explained by mitochondrial dysfunction, Nurr1 loss might contribute to the dysfunction.

1.4.2 Nurr1 in Parkinson's disease

Abnormalities in the Nurr1 gene seem to be a risk factor for PD according to several studies (Grimes et al., 2006; Wei-dong Le et al., 2003; Weidong Le et al., 2008; Zheng et al., 2003). Mutations and polymorphisms have been linked to both sporadic and familial PD. These genetic variations in the Nurr1 gene were found to decrease Nurr1 mRNA levels in lymphocytes (Weidong Le et al., 2008). It is postulated that the variations could also affect Nurr1 expression in DA neurons in the brain and cause dysfunction of DAergic system in PD (Jankovic et al., 2005; Wei-dong Le et al., 2003). Post mortem tissue analysis has revealed decreased Nurr1 levels in the SN in deceased PD patients. This decline was correlated with loss of TH. Also Nurr1 was significantly decreased in nigral neurons containing α-synuclein inclusions but not in neurons that were inclusion free (Chu et al., 2006). Nurr1 expression in peripheral lymphocytes is significantly decreased in PD (Weidong Le et al., 2008). This suggests that Nurr1 could be used as a peripheral biomarker for early diagnosis of PD.

1.4.3 The Nurr1 knock-out model of Parkinson's disease

As mentioned before *Nurr1*$^{-/-}$ knock-out (KO) mice fail to differentiate midbrain DA neurons and die soon after birth. On the other hand heterozygous *Nurr1*$^{+/-}$ mice developed DA neurons but the numbers of neurons were reduced in old mice compared to wild type (WT) and locomotor activity was altered parallel to that. In addition, the KO animals were more susceptible to toxic stress than WT animals (Jiang et al., 2005).

To exclude the option that the increased DAergic vulnerability was caused by defects in the developmental stages, another type of Nurr1 KO model was generated where a conditional

ablation of the Nurr1 gene after maturation of the midbrain DA neurons was performed (Decressac et al., 2013). It allowed the animals to develop healthy DA neurons, exposed to a normal activity of Nurr1, that started to degenerate slowly after ablation of the Nurr1 gene and resulted in a progressive dysfunction of the DAergic system (Blaudin de Thé, Rekaik, Prochiantz, Fuchs, & Joshi, 2015).

Kadkhodaei et al managed to achieve a complete ablation by tamoxifen treatment of conditional Nurr1 gene-targeted mice expressing the $CreER^{T2}$ enzyme under the DAT gene regulatory sequence (Kadkhodaei et al., 2013). Ablation in five weeks old mice resulted in a decreased expression of TH, VMAT2 and DAT four weeks post ablation, but no loss of cell bodies and the cellular integrity of DA neurons remained intact 11 months after ablation (Kadkhodaei et al., 2013).

Dopamine levels were dramatically decreased in the striatum and NAc and locomotor tests, performed 3-5 months or 11 months after ablation, resulted in a significant motor impairment (Kadkhodaei et al., 2013). Progressive reduction in fiber density was observed in striatum and GP 4 months and 11 months after Nurr1 ablation. Gene expression assays reviled significantly reduced expression in 90% of all nuclear-encoded genes involved in oxidative respiration (Kadkhodaei et al., 2013). These results indicate that Nurr1 is important to maintain sufficient respiratory function in DA neurons. The model recapitulates the early stages of PD and suggests that age dependent decrease in Nurr1 expression might contribute to the pathology of PD.

1.5 MALDI Mass Spectrometry Imaging

Mass Spectrometry Imaging (MSI) is a technique that allows direct tissue analysis and visualization of a large number of molecules. In MSI a mass spectrometric analysis is performed on a tissue section, where a multitude of measurements are taken from the sample slice within a predefined region. The results give a mass spectrum for each individual measuring spot and a two dimensional distribution map is generated (Balluff, Schöne, Höfler, & Walch, 2011).

MSI can directly localize a wide range of biomolecules simultaneously and no specific target handling is needed (Ye, Wang, Greer, Strupat, & Li, 2013). This makes it a useful tool in the search for new biomarkers.

1.5.1 General work flow of MSI

The basis of MSI analysis is to separate different molecules by their mass-to-charge (m/z) ratio. The process is divided into three parts: desorption and ionization of analytes, separation of ions and ion detection (Cameron, 2012). Several different desorption and ionization techniques have been developed. The most commonly used techniques are matrix assisted laser desorption/ionization (MALDI), secondary ion mass spectrometry and desorption electrospray ionization. After analytes have been desorbed and ionized they are separated by their m/z ratio in a mass analyzer. A variety of physical strategies can be used to separate the ions. Time-of-flight (TOF), ion trap and quadrupole mass analyzers are examples of analyzers used in this purpose. At the end, a detector is responsible for quantification of the ions and generating a mass spectrum which can then be analyzed using specific software developed and optimized for the instrument (Cameron, 2012).

MALDI is a soft ionization technique that desorbs and ionizes molecules that have been mixed with a matrix. The technique first emerged 1988 (Karas & Hillenkamp, 1988) and was utilized in MSI about ten years later (Caprioli, Farmer, & Gile, 1997). Since then it has been developed and optimized making it more sensitive and robust. It has been applied to the clinical setting in investigating tumors and to drug development for examining drug distribution (Balluff et al., 2011).

The method uses short ultraviolet laser pulses to desorb and ionize molecules that have been mixed with a matrix. The matrix is a small organic molecule, usually an organic acid, which can absorb energy at the wavelength that the laser emits and facilitates ionization. The matrix is sprayed onto a sample and allowed to dry. During drying the matrix molecules and analytes form co-crystals. Then the sample is exposed to very short laser pulses resulting in desorption and ionization of analytes (Walch, Rauser, Deininger, & Höfler, 2008). With special preparation, MALDI allows detection of molecules with masses up to 70 kDa (Meding & Walch, 2013) and scientists have achieved to reach a lateral resolution down to 5µm (Römpp & Spengler, 2013)

1.5.2 Sample preparation

The basic sample preparation procedure can be divided into four parts. They are sample handling, staining, tissue treatment and matrix application (Norris & Caprioli, 2013). The second and third parts are optional and depend on the purpose of the experiment.

1.5.2.1 Sample handling

In MALDI-MSI it is important to preserve both the histological and molecular integrity while handling the sample. The time interval from harvesting the sample until it is preserved in a frozen environment must be minimized to prevent degradation and delocalization of analytes (Goodwin, 2012). The first step in the sample collection is to snap freeze the sample using a cryogen such as liquid nitrogen, pentane or hexane or dry ice. Then it can be stored in -80°C for the minimum of 1 year without affecting the quality of the MALDI-MSI result (Norris & Caprioli, 2013).

Tissue sectioning is performed in a cryotome and needs to be done in a correct manner. It should be performed at an optimal temperature and thickness to produce high quality samples for imaging. Tissue thickness for MALDI-MSI is between 3-20 µm and the recommended temperature for cutting unfixed tissues are usually between -30°C and -12°C (Norris & Caprioli, 2013) Both the cutting temperature and the tissue thickness depend on the type of tissue that is being cut (Norris & Caprioli, 2013). After cutting, the section is thaw mounted onto a surface that has been cooled down to the same temperature as the section. The section is carefully placed on the surface and then it is slowly warmed from the other side of the surface. For MALDI-TOF this surface is usually a conductive glass slide is required for accelerating the ions in the ion source of the mass spectrometer (Norris & Caprioli, 2013).

1.5.2.2 Staining

Staining of tissue samples is an optional step in preparation and sometimes necessary to confidently identify and target regions of interest. Staining can be applied to samples either prior to application of matrix or after by washing off the matrix after MALDI data has been obtained (Chaurand et al., 2004). Staining prior to matrix application gives the best insurance that the correct regions of interest are targeted. However it might affect the results of the MALDI-MSI data because undesired changes to molecular composition can occur during the staining procedure (Chaurand et al., 2004). Hematoxylin and eosin (H&E) staining is a commonly used histological staining procedure. It has been found that H&E staining of sections significantly compromise the quality of MALDI data relative to unstained control (Chaurand et al., 2004). However it can be applied to samples after MALDI-MSI acquisition to obtain a histological references (Deutskens, Yang, & Caprioli, 2011).

1.5.2.3 Tissue treatment

Tissues can be pretreated in several ways to enhance the analytes of interest before application of matrix. The most common procedures are on tissue derivatization, on tissue digestion and tissue washing to remove salts and contaminants. These procedures can give significant gain in sensitivity for the analytes of interest and are sometimes essential for obtaining a signal (Norris & Caprioli, 2013).

1.5.2.4 Matrix application

The role of the matrix is to absorb laser energy and transfer the analyte to gas phase while promoting ionization. The matrix should be selected in regard to the analytes of interest. It is usually dissolved in a mixture of an organic solvent and water (Norris & Caprioli, 2013). Matrix application can be performed manually or by using a robotic sprayer. It is important that the coating is homogenous and the crystal size is small. It is important to avoid wetting during application of tissue because the matrix solvent might delocalize the analytes (Eriksson, Masaki, Yao, Hayasaka, & Setou, 2013).

1.5.2.5 Data acquisition and analysis

The MALDI-MSI platform consists of three components; the instrument hardware (the MALDI source and mass analyzer), the software platform designed for acquisition of MSI data and lastly the software for visualization and analysis. Numerous academic groups and companies have developed software and instruments for MALDI-MSI. These platforms have their specific capabilities so the instrument should be chosen by considering what capabilities are important for the MSI application (Norris & Caprioli, 2013).

1.5.2.6 Spatial resolution

Spatial resolution has an impact on the molecular information that can be obtained from MSI. Higher resolution gives more detailed biological information by providing information on a cellular level and cell layers and clusters of cells can be imaged (Römpp & Spengler, 2013). However higher resolution negatively affects other parameters such as sensitivity, sample throughput and the amount of data that has to be managed (Norris & Caprioli, 2013). So balance should be found between these parameters with the purpose of the experiment in mind. The laser beam diameter and pitch between the ablation spots specify the spatial resolution. Resolution ranging from 200µm to 20µm is most commonly used in MALDI-MSI (Norris & Caprioli, 2013).

1.5.3 Imaging Neurotransmitters

MALDI-MSI has been used to detect peptides, proteins, lipids, metabolites and pharmaceuticals for some time but it was recently applied to image neurotransmitters (NTs) (Shariatgorji et al., 2014; Sugiura, Zaima, Setou, Ito, & Yao, 2012; Ye et al., 2013). Insight into changes in NTs concentrations can deepen our understanding of the molecular mechanism of neurological diseases.

Traditional neuroimaging techniques are based on immunohistochemical methods. They image antibodies against targets or target specific enzymes involved in synthesis of NTs. Immunohistochemical imaging have a few drawbacks, sample preparation can be troublesome, highly target specific antibodies can be hard to obtain, a limited number of molecules can be detected simultaneously and discovery of unknown molecules is impossible since you have to have a known target (Ye et al., 2013). By using MALDI-MSI it is possible to directly detect NTs and their metabolites from their m/z ratio and several NTs can be detected in each run.

Imaging NTs with MSI can be troublesome. Because of their low molecular weight signals can be mixed with high abundance matrix derivative peaks. Also physiological concentration are low which decreases sensitivity (Ye et al., 2013). Some NTs have poor ionization efficiency (Shariatgorji et al., 2014). Shariatgorji et. al. recently published a method that addresses these problems and enables visualization of several NTs and metabolites. NTs that contain primary amines were derivatized with 2,4-diphenyl-pyranylium (DPP). The derivatization made the compounds positively charged and enabled the imaging of dopamine, GABA and serotonin as well as 3-MT, a dopmamine metabolite (Shariatgorji et al., 2014).

The matrix α-cyano-4-hydroxycinnamic acid (CHCA) is one of the most used matrixes in MALDI-MSI. The use of it is complicated by interference from matrix ion clusters and fragments peaks that mask signals of low molecular weight compounds. They cover the mass range of acetylcholine (ACh). The application of the D^4-deuterated CHCA (DCHCA) shifts these interfering signals to reveal the signal for ACh (Shariatgorji et al., 2012).

Applying these methods to a PD model might provide valuable information about changes in neuronal communications in the disease.

2. OBJECTIVES

2.1 Primary objective

To use MALDI-MSI to simultaneously image multiple neurotransmitters and metabolites in brain sections of a progressive Parkinson‘s disease model (Nurr1 knock-out) mouse model as well as control animals.

To investigate how Parkinson‘s disease affects neurotransmitters concentration and distribution by performing a relative quantification of the imaged neurotransmitters in selected structures in the brain. Also to examine if treatment with the dopamine agonist apomorphine affects the levels of neurotransmitters compared to saline treated.

2.2 Secondary objective

To apply a histological staining method to the samples after MALDI-MSI measurement and implement it to the MALDI data.

3. MATERIALS, INSTRUMENTS AND METHODS

3.1 Materials

Table 1. Material, manufacturer and catalogue or batch number

Material	Manufacturer	Catalogue or batch
Matrices		
Acetonitrile	Merck	I754830 441
9-Aminoacridine hydrochloride monohydrate (9-AA)	Sigma-Aldrich	09820CEV
d-α-cyano-4-hydroxycinnamic acid (DCHCA)	Ubichem	631285005
LiChorsolv water	Merck	Z0353733 530
Derivatization		
4-(anthracen-9-yl)-1-methylpyridinium (ANTH-MP)	Prepared in-house	-
2,4-diphenyl-pyranylium (DPP)	Prepared in-house	-
Calibration		
α-cyano-4-hydroxycinnamic acid (CHCA)	Sigma Aldrich	SHBB2063V
2,5-Dihydroxybenzoic acid (DHB)	Merck	S6313645 228
Sinapic acid (SA)	Fluka	BCBD0956V
9-Aminoacridine hydrochloride monohydrate (9-AA)	Sigma-Aldrich	09820CEV
Histological/H&E staining		
Acetic acid >90%	Scharlau	67345
HTX stain solution	Mayers	251188
Eosin	VWR International	ZC218326 428
Ethanol 99,7%	Solveco	6088068
Ethanol 96%	Solveco	6089139
Mounting medium	Pertex	1711055
Xylene	J.T. Baker	1425806866

3.2 Instruments and equipment

Table 2. Instrument and equipment for sample preparation and analysis

Instrument/Equipment	Manufacturer	Version/Series
Tissue preparation		
Desiccator	Bel art	Space saver
Glass slides, ITO covered	Bruker	Glass slides for MALDI imaging
Matrix application and derivatization		
Automated sprayer	HTX-Imaging	TM-Sprayer
Conical Tube	BD Falcon	15 mL
Pipette (100-1000 µL)	Mettler Toledo	Volumate
Pipette (0,1-2,0 µL)	Rainin	Pipet-Lite XLS
Pipette tips (100-1000 µL)	Gilson	Diamond
Pipette tips (0,1-2,0 µL)	Mettler Toledo	Precision pipette tips
Scale	Mettler Toledo	Sartorius
Sonicator	VWR	USC300TH
Vortex	Labora	Vortex-Genie 2
MALDI-MSI analysis		
MALDI-TOF/TOF analyzer	Bruker	Ultraflextreme
Software and website		
Brain atlas	Allen Institute for brain science	Allen brain atlas
FlexControl	Bruker	Version 3.4
FlexImaging	Bruker	Version 4.1
MsIQuant	In-house developed software	Version 2
IsotopePattern	Bruker	Version 2.0
Histological staining		
Cover slips	Mentzel-Gläser	24x24 mm and 22x 55 mm

3.3 Methods

3.3.1 Animal generation and treatment

For generation of conditional KO animals, Nurr1 floxed mice were crossed with mice harboring a tamoxifen inducible Cre ($CreER^{T2}$) enzyme linked to the DAT gene regulatory sequences in an artificial bacterial chromosome (BAC-DAT-Cre^{ERT2}) (Engblom et al., 2008; Kadkhodaei et al., 2009, 2013). Homozygous Nurr1 floxed mice with a single copy of the BAC-DAT$CreER^{T2}$ transgene ($cNurr1^{DATCreER}$) were generated and used in this experiment and homozygous Nurr1 floxed mice carrying no copies of the BAC-DAT$CreER^{T2}$ transgene were used as control.

At the age of 5 weeks the animals were treated with tamoxifen. Two milligrams twice a day for 5 days were injected intraperitoneally in a 20 mg/ml ethanol solution (Kadkhodaei et al., 2013).

The animals from the sagittal tissue samples were untreated but those from coronal samples were treated either with APO or SAL 1mg/kg once per day for 4 weeks. Animals were sacrificed by decapitation 15 min after the last injection. Brains were quickly dissected and put in isopentane for snap freezing for 15-20 s. Then they were wrapped in tin foil and put into a freezer (-80°C). Animals referred to as adult were 4-7 months old when sacrificed and those referred to as old were 11 months or older when sacrificed. The experiments were performed in agreement with the European Communities Council Directive of November 24, 1986 (86/609/EEC) on the ethical use of animals and were approved by the local ethical committee at Karolinska Institute.

3.3.2 Tissue handling

Sagittal and coronal brain tissue sections were obtained from Karolinska Institutet in Stockholm. Sections had been cut with a thickness of 12 µm, were thaw mouthed onto conductive indium tin oxide (ITO) slides and stored at -80°C until transportation to the lab in Uppsala. Samples were transported on dry ice and put into freezer at -80°C upon arrival. Prior to further tissue preparation samples were transported from freezer on dry ice and put into a desiccator for 30 min.

3.3.3 Matrix application and derivatization

Four different application solutions were used, two matrixes and two different derivatization agents. They were applied with an automated matrix sprayer, the HTX-sprayer. It transfers

heat to the matrix solution to increase absorption into the tissue and uses nitrogen to focus the spray and trying time. The sprayer controls parameters such as heat and flow rate of the matrix, velocity of the spray nozzle, size and shape of the area to be sprayed and number of spraying passes. Different settings are needed for each application and are listed in Table 3 Nitrogen pressure was fixed at 6 psi for all the settings.

Table 3. HTX-sprayer settings for matrix application and derivatization.

	concentration	**solvent**	**temperature**	**flowrate**	**passes**
9-AA	5 mg/mL	70% ACN	90°C	0.070 mL/min	8
DCHCA	5 mg/mL	50% ACN 0,2% TFA	90°C	0.070 mL/min	6
DPP	2,3 mg/mL	70% MeOH 0,06% TEA	80°C	0.080 mL/min	30
ANTH-MP	1,8 mg/mL	70% ACN	80°C	0.080 mL/min	30

Derivatization with DPP requires an incubation step after HTX application. The slides taped to the inside of a cover of a petri dish that contained 4.0 mL of 50% methanol. The covered petri dish was kept moving on a rocking device for 3-5 min. Then the slides were dried with nitrogen gas. This was repeated three times.

3.3.4 MALDI-MSI analysis

After matrix application slides were scanned to obtain an optical image to use for marking teaching points to the method of the MALDI run. The MALDI-MSI was performed using an Ultraflextreme TOF/TOF mass spectrometer (Bruker Daltonics, Bremen, Germany). Analysis was performed in positive ion reflection mode except for the experiments using 9-AA as matrix; they were run in negative ion reflection mode. Acquisition was set up using FlexControl (Bruker Daltonics, Bremen, Germany) and FlexImaging (Bruker Daltonics, Bremen, Germany). Spatial resolution was set to 100 µm for coronal sections and 120 µm for sagittal sections. Regions for imaging were selected in randomized order to reduce any bias arising from factors such as variation in the mass spectrometer sensitivity and matrix degeneration.

3.3.5 Data handling

After MALDI-MSI run data was loaded into the FlexImaging software. Some pre-analysis was performed on raw data such as marking peaks by adding mass filters and comparing individual spectra for each tissue section. This was done to get a quick overlook of discrepancies between groups.

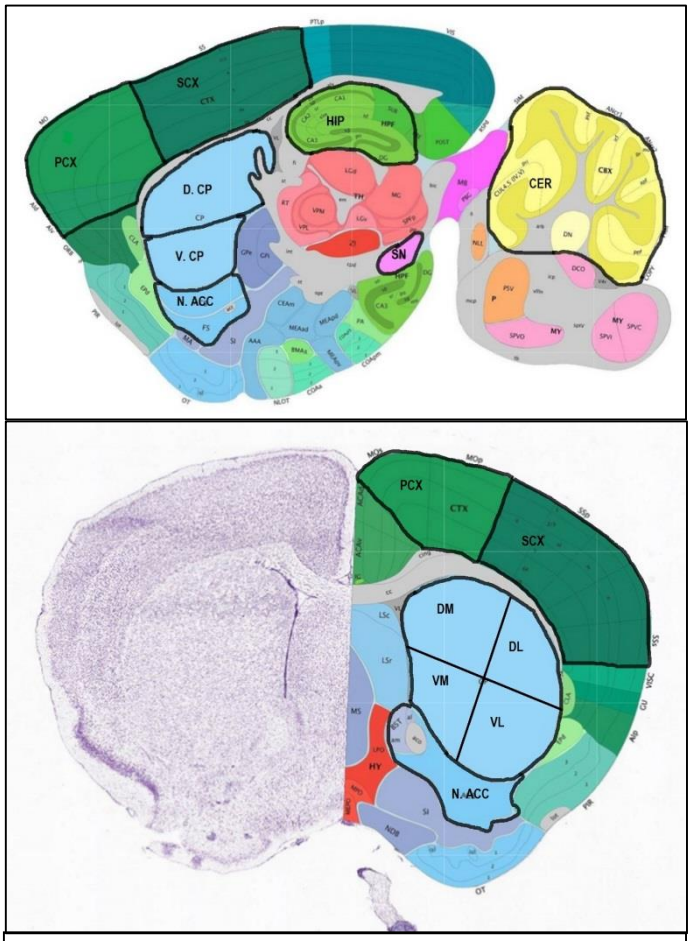

Figure 2. Brainstructures used in the relative quantification of neurotransmitters. The areas are drawn onto the sample picture with black borders.

Raw data was exported from FlexImaging and converted into msIQuant data. The msIQuant software allows extraction of intensity values for written regions of interest (ROI). The following brain structures were used in the comparison of NT in sagittal sections; dorsal caudate putamen (dCP), ventral caudate putamen (vCP), NAc, HIP, cerebellum (CER), prefrontal cortex (PCX), sensorimotor cortex (SCX) and SN. For the coronal brain tissue sections the structures PCX, SCX and CP were used. In addition the CP was divided into four parts; dorsal medial (DM), dorsal lateral (DL), ventral medial (VM) and ventral lateral (VL) to look at the distribution of dopamine inside the CP. The regions were drawn onto optical images that were adjusted and aligned to fit the imaging results. An interactive mouse brain atlas (Allen Institute for Brain Science, 2015) was used as reference to the brain regions and the level in the brain the sections belonged to. Figure 2 shows the ROIs that were drawn.

The analytes of interest were identified with the help of the IsotopePattern (Bruker Daltonics, Bremen, Germany, version 2) software that calculates exact m/z values based on molecular formulas. After the regions had been drawn the m/z values of interest were selected and the

msIQuant software extracted numbers for ion intensity for each region of interest. The results were presented as arbitrary units (a.u.) per unit area (mm^2) and those numbers were used for further analyzation.

3.3.6 Histological staining with hematoxylin and eosin

Since region specific data is being generated it is important to mark the ROIs in a correct manner. Identifying brain regions form looking at an optical image after matrix application can be troublesome. Thus a histological staining procedure using hematoxylin and eosin (H&E) was applied to the samples after the MALDI-MSI measurement.

3.3.6.1 Washing off matrix

The matrix was washed off by covering in 97% ethanol in a petri dish for 30 s and then directly put in 50% ethanol for additional 30 s. The petri dish was kept gently rocking manually to get movement on the dissolving matrix. Next the slides were covered in water for at least 2 min prior to staining.

3.3.6.2 Staining

Samples were delivered from the water bath to the hematoxylin solution. All samples were carried out in hematoxylin for 3 min then they were put in tab water for at least 10 min.

Staining with eosin can be more troublesome because if the sample is kept in the solution too long it might take too much color and vice versa. Table 4 lists the methods that were tested for eosin staining to optimize the procedure.

Table 4. Methods tested for staining with eosin.

Method	Eosin solution	Time in solution
1	100 mL of 1,5% eosin with 0,5mL of 90% acetic acid	10
2	100 mL of 70% ethanol with 3 mL of solution 2	30
3	100 mL 0,2% eosin	30
4	100 mL 0,2% eosin	60
5	100 mL of 1,5% eosin	40
6	100 mL of 1,5% eosin	30

Directly after eosin the samples were quickly dipped in alcohol following the procedure:

70% ethanol for 3 sec, repeat for 3 sec, 96% ethanol for 30 sec, absolute ethanol for 5 min. Then the samples were covered in xylene for 5 min and repeated for 5 additional min. The samples were mounted with a mounting medium, covered with cover slips and allowed to dry overnight.

4. RESULTS

4.1 MALDI-MS imaging of neurotransmitter in sagittal brain sections

The experiments in this work generated a very large amount of data and images and only the most important results are presented in this thesis.

4.1.1 MALDI-MSI following DPP derivatization

Results from MALDI-MSI of neurotransmitters following derivatization with DPP are shown in Figure 3. Dopamine (DA) was detected at m/z 368.16. The signal from DA is strongest in the caudate putamen (CP) and reaches down to the ventral part of the striatum and to the olfactory tubercle. The intensity was highest in the wild type (WT) adult animals and decreased in the following order WT old, knock-out (KO) adult and KO old.

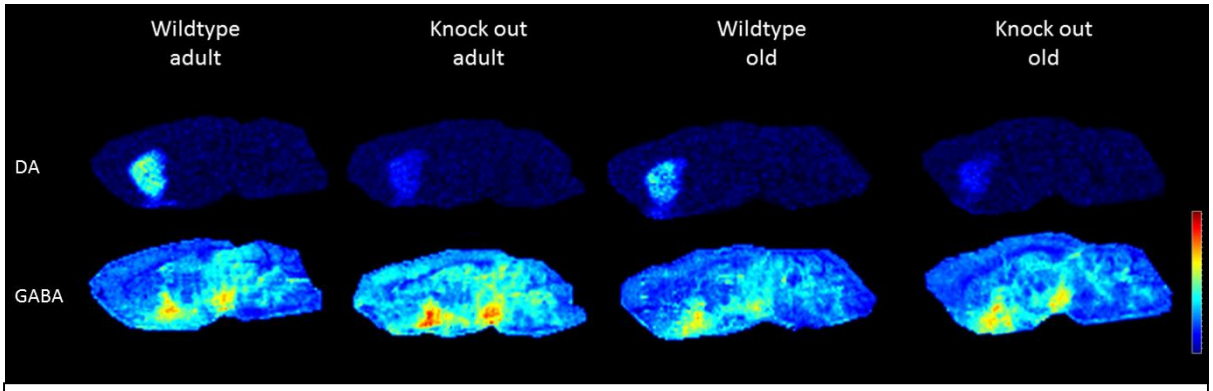

Figure 3. MALDI-MSI of mouse brain tissue section following DPP derivatization. One brain section per group is displayed. Signal intensities are indicated using a rainbow scale. Spatial resolution: 120 µm. The images are TIC normalized.

GABA, which was detected at m/z 318.14, exhibited a high signal and was detected in most structures of the brain. It was most abundant in the SN and in medial septum-diagonal band (MSDB) region (Shariatgorji et al., 2014). The lowest signals were in corpus callosum and in the white matter of the cerebellum.

4.1.2 MALDI-MSI with DCHCA

MALDI-MSI with the non-deuteraded α-cyano-4-hydroxycinnamic acid (CHCA) is often complicated by interference from matrix ion clusters and fragments peaks that mask signals of low molecular weight compounds. The D^4 deuterated CHCA shifts these peaks and clusters and reveals the signal for the neurotransmitter acetylcholine (ACh) (Shariatgorji et al., 2012). The choline α-GPC was also detected with DHCHA. The Peaks were located at

m/z 146.13 for ACh and 258.15 for α-GPC. ACh showed the highest intensity in the cortex and frontal part of the brain. α-GPC was low in the parts where ACh was high (Figure 4).

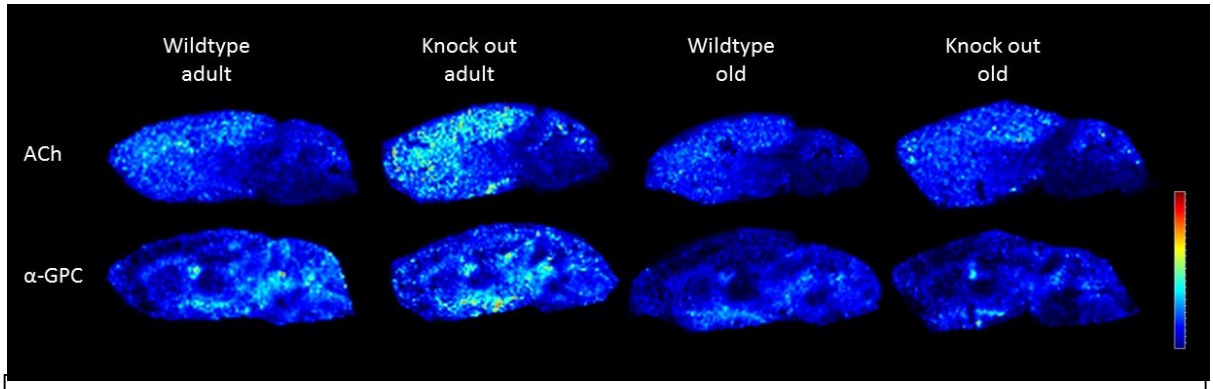

Figure 4. MALDI-MSI of mouse brain tissue section following DCHCA application. One brain section per group is displayed showing the distribution of ACh and α-GPC. Signal intensities are indicated using a rainbow scale. Spatial resolution: 120 µm. The images are TIC normalized.

4.1.3 MALDI-MSI with 9-AA in negative mode

MALDI-MSI was performed in negative mode to image the negatively charged amino acids glutamate, glutamine and aspartate and they were detected at m/z 146.03, 145.06 and 132.01 respectively. The resulting images are shown in Figure 5. The analytes are distributed through the whole tissue and they all show highest intensity in the cerebellum.

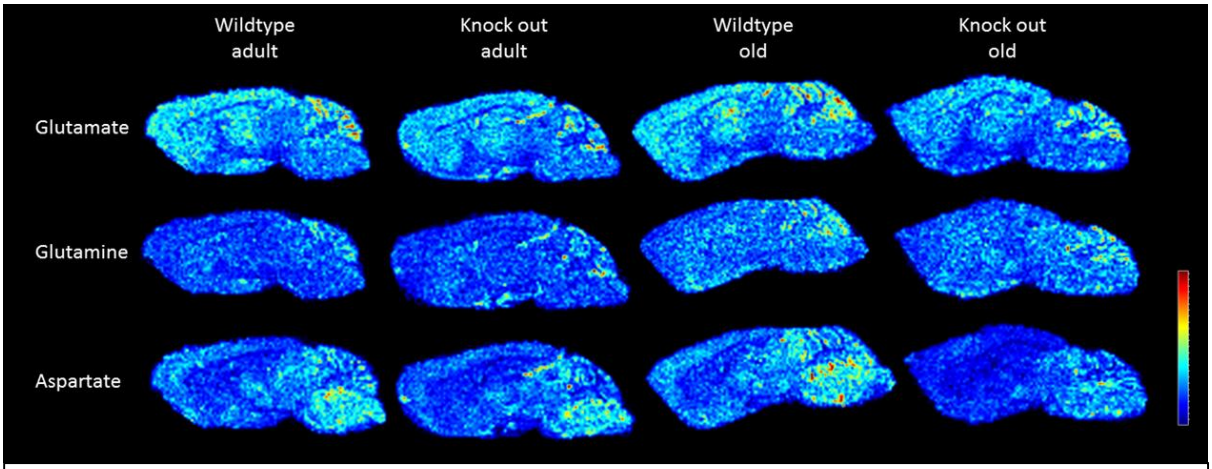

Figure 5. MALDI-MSI of mouse brain tissue section following 9-AA application performed in negative mode, displaying the distribution of Glu, Gln and Asp (one brain section per group). Signal intensities are indicated using a rainbow scale. Spatial resolution: 120 µm. The images are TIC normalized.

4.2 Hematoxylin and eosin staining of tissue sections

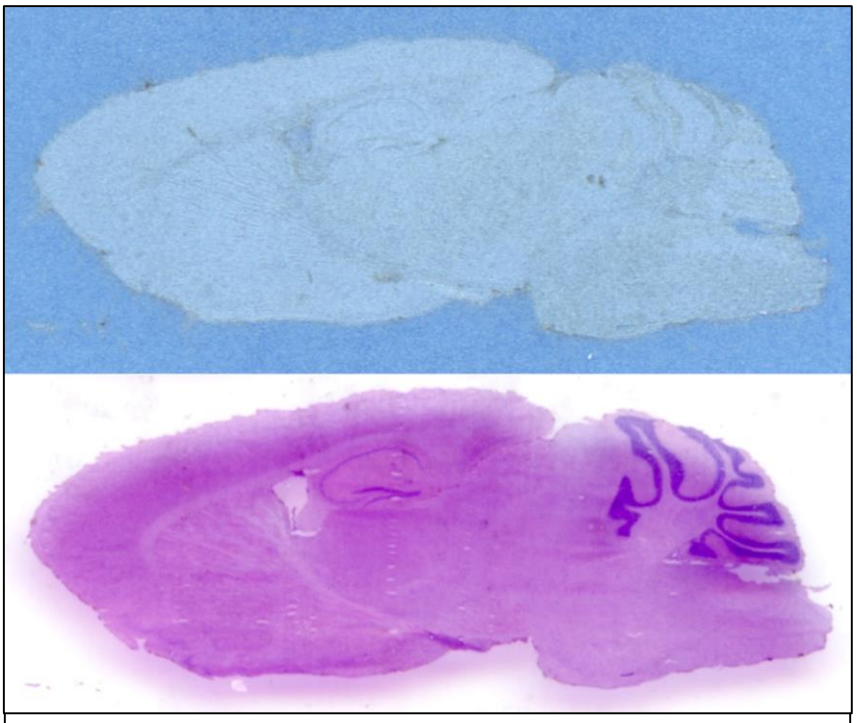

Figure 6. Sagittal brain tissue section with DCHCA matrix (above) and after H&E staining (below).

After MALDI-MSI measurements were performed the tissues were stained using an H&E protocol. Several different eosin solutions were tested and the best result came from Method 2 (Table 4).

Figure 6 showes a sagittal tissue section before staining, covered with DCHCA matrix and the same tissue after staining. Many of the structures became clearly visible after staining. The CER and HIP were more visible especially the inner structures. The CP was easier to recognize as it was framed by the lighter colour of the fiber tracts surrounding it. However it was still difficult to discover the border between CP and the NAc. It was interesting to note that the DPP samples absorbed more red color although the same protocol was followed for all samples (Figure A in Appendix I).

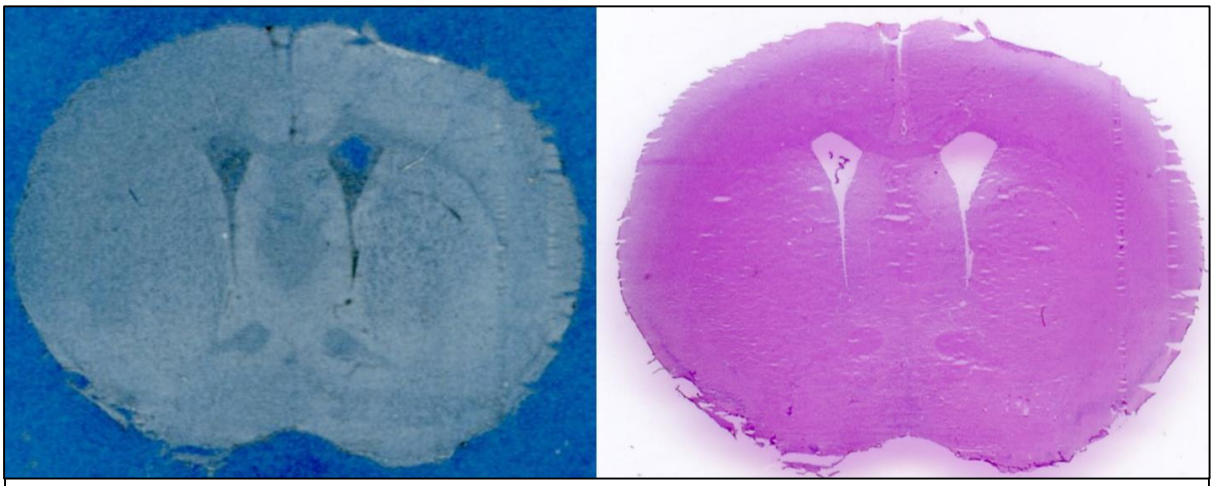

Figure 7. Coronal brain tissue section with DCHCA matrix (left side) and after H&E staining (right side).

Since the staining of sagittal tissue sections were succsessful the same method was applied to the coronal samples. Figure 7 displays a coronal tissue section before and after staining. The coronal sections did not show as good results as for the sagittal tissues. Damages that occurred during cutting the tissue sections like folded parts and scratches became more visible.

4.3 Relative quantification of neurotransmitters in sagittal brain tissue sections

The numbers were extracted from the data as the sum of intensities for every spot in the region of interest (ROI) divided by the surface area of the ROI (SUM/area) and were in arbitrary units per mm^2. Adult WT animals exhibited the highest intensity of DA and were therefore used as control (set to 100%) when comparing levels of NTs between the animal groups.

4.3.1 Dopamine

Figure 8 shows results from relative quantification of DA. One of the subjects in the KO old group exhibited a relatively high signal compared to the other subjects in the group and multiplied the standard error of the mean (SEM) and was therefore excluded from the analysis.

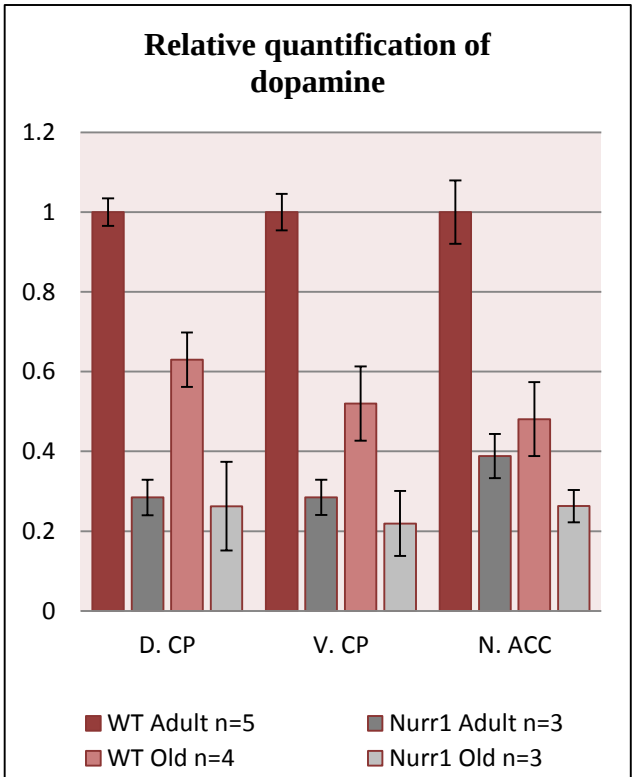

Figure 8. Relative quantitation of DA with average values for WT adult set as one. The SEM is presented on the bars.

Since DA signal was nearly exclusively shown in the striatum it was divided into three parts for examination. The three parts were the dCP, the vCP and the NAc. The KO animals exhibited around 70% reduction in all regions and the older KO animals were slightly lower than the adult ones. Old WT animals showed a decrease about 50% in the ventral part of the striatum (vCP and NAc) and 40% in the dorsal CP.

4.3.2 Acetylcholine

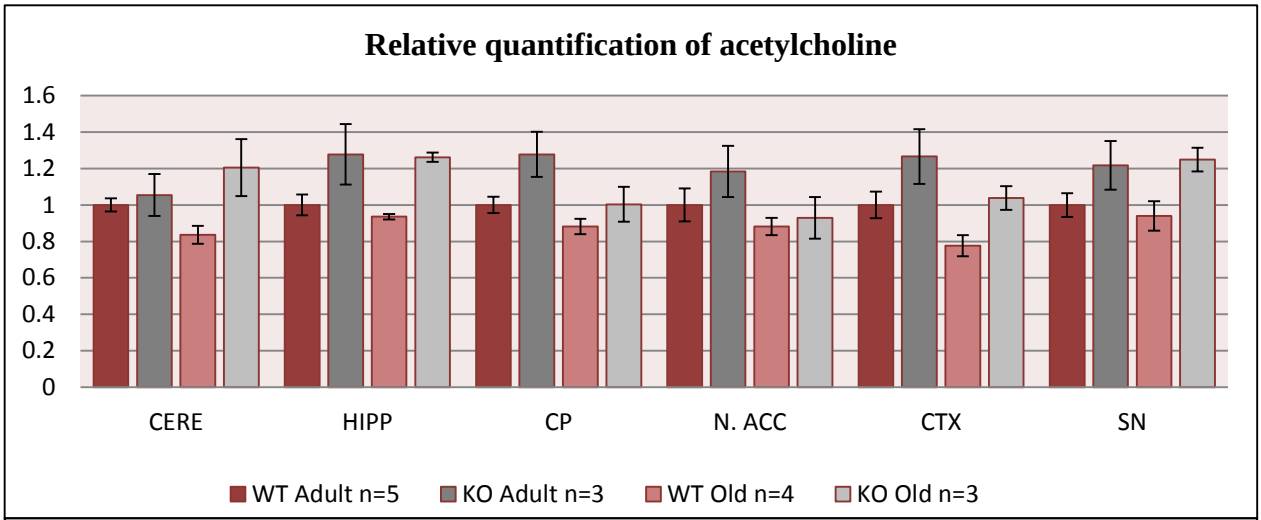

Figure 9. Relative quantitation of ACh in six different structures of the brain. Average values for WT adult are set as one. The SEM is presented on the bars.

The KO animals exhibited higher ACh than the WT animals when comparing the two genotypes in the same age groups. This was quite consistent in all brain regions (Figure 9).

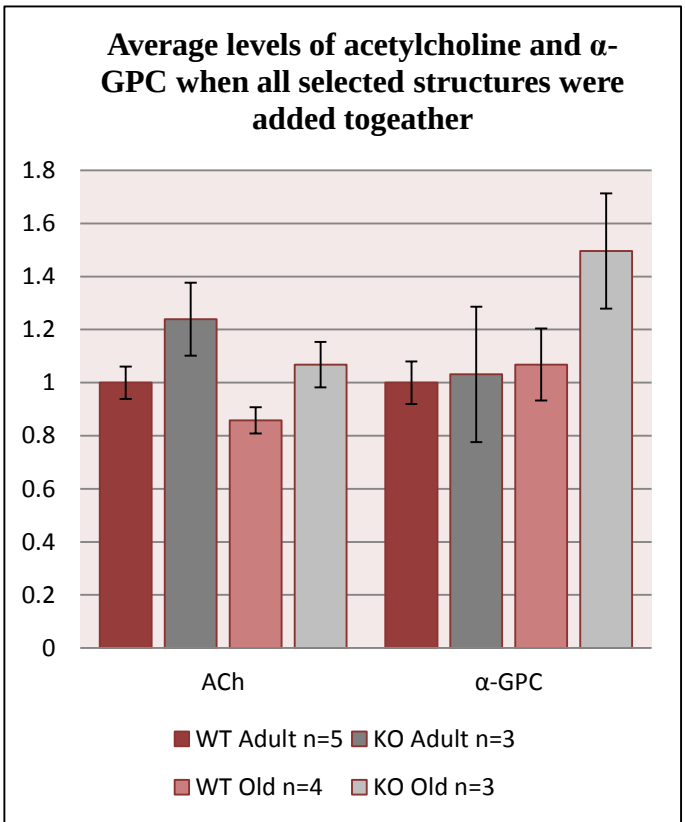

Figure 10. Relative quantification of ACh and α-GPC. The sum of the intensities for each molecules for all selected structures. The SEM is presented on the bars. WT adult is set as one.

When intensities for all selected structures were added the KO animals showed about 24% increase in ACh for both age groups (Figure 10).

To examine α-GPC in contrast to ACh it was the sum of the average intensities for all ROIs were calculated are presented in Figure 10. α-GPC was highest in adult WT animals with a 50% increase. In the NAc it exhibited more than twofold increase in old KO compared to old WT animals with relatively low variance.

4.3.3 Glutamate, glutamine and aspartate

The negatively charged amino acids aspartate (Asp), glutamine (Gln) and glutamate (Glu) did not show any region specific difference. Therefore, to clarify the results, the intensities for all structures drawn onto the tissues were summed and used in the comparison (Figure 11). Both Glu and Asp decreased in the order WT adult, KO adult, WT old and KO old. In contrast Gln increased in the same order. The variation was low.

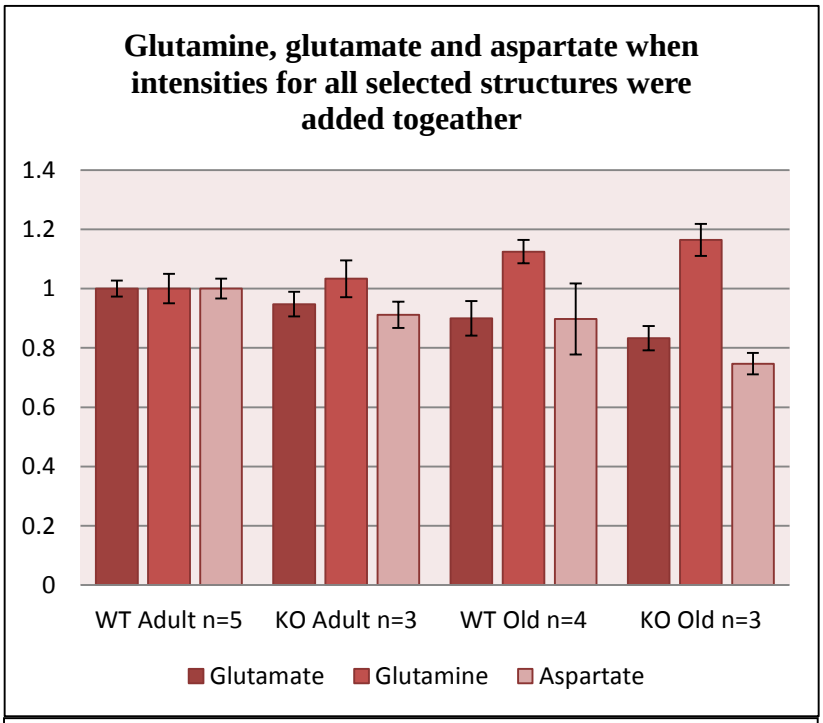

Figure 11. The sum of the intensities of glutamine, glutamate and aspartate for all selected structures with WT adult set as one. The SEM is presented on the bars.

4.4 MALDI-MS imaging of neurotransmitters in coronal brain tissue sections

To examine the treatments effect of the dopamine agonist apomorphine (APO) on neurotransmitters, APO treated wild type (WT) and knock-out (KO) animals were compared to saline (SAL) treated WT and KO animals. The effect of knocking out the Nurr1 gene was also examined by comparing the different genotypes that had been given the same treatment. All animals in this experiment were adult (4-7 months old).

4.4.1 MALDI-MSI following ANTH-MP derivatization

For this experiment the anthracene analog ANTH-MP was used for derivatization. It has a reactive methylpyridinium group that reacts with monoamines and alcohol groups. It adds a positive charge to the molecule and increases the weight of the molecule.

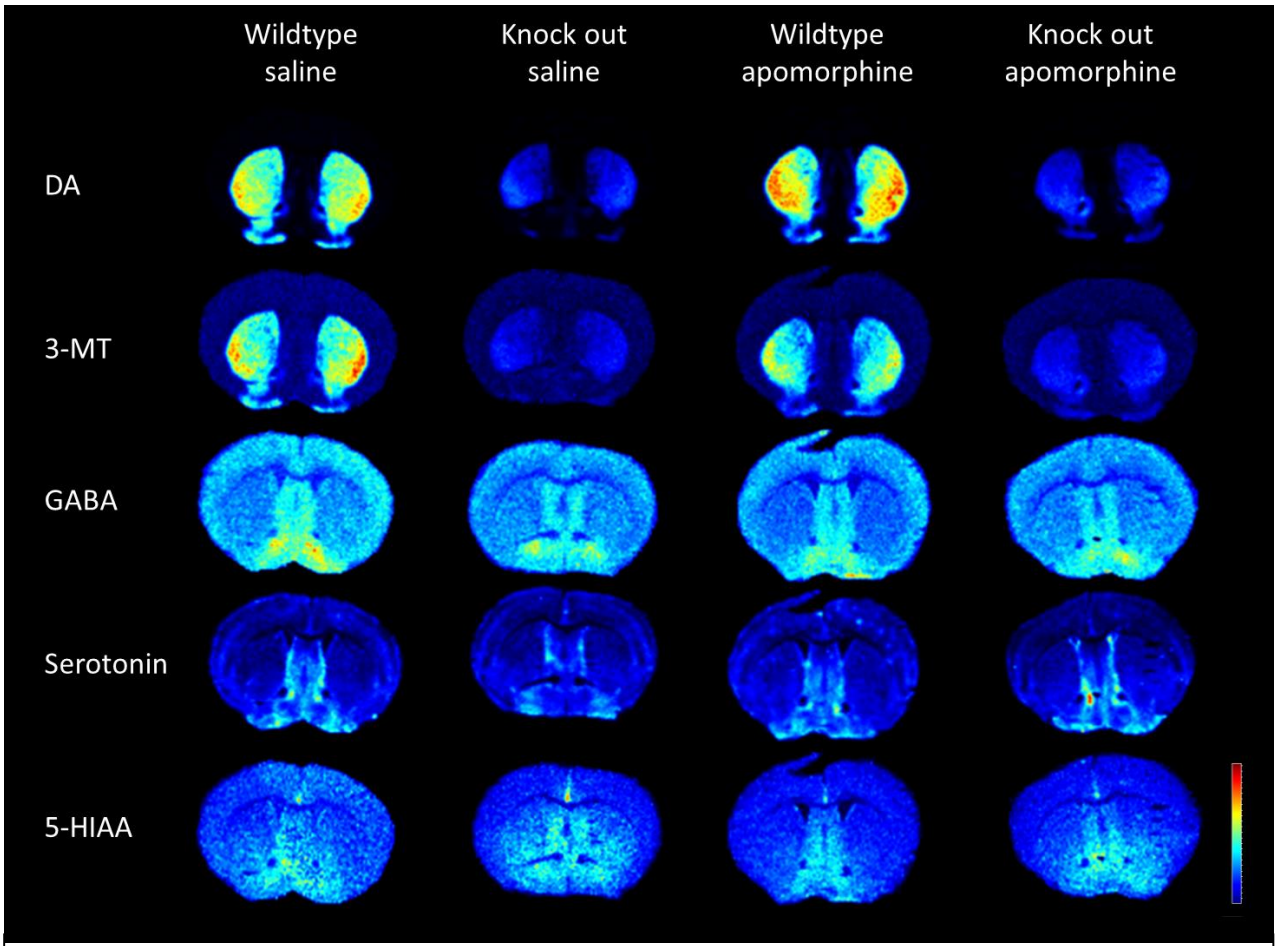

Figure 12. MALDI-MSI of coronal mouse brain tissue sections following ANTH-MP derivatization. One brain section for each group is displayed. Signal intensities are indicated using a rainbow scale. Spatial resolution: 100 µm. The images are TIC normalized.

Dopamine was detected with high intensity. Three peaks were observed for DA due to the derivatizing agent (the singly, doubly and triply derivatized analogues at m/z 421.3, 674.4 and 941.6 respectively). The doubly derivatized analogue exhibited the highest intensity and is displayed in Figure 12. DA was predominantly localized in the striatum and was highest in the ventral lateral part. DA was also visualized in the olfactory tubercle.

The O-methylated DA metabolite 3-MT was detected at m/z 435.3 and 688.5 for the singly and the doubly derivatized. The doubly derivatized exhibited the stronger signal and is displayed in Figure 12. It had the same distribution as DA although it showed a much weaker signal than DA.

The inhibitory neurotransmitter GABA was detected at m/z 371.3 and is displayed in Figure 12. The signal was partly overlapping with an isotopic signal from a peak at m/z 370.3 but that signal was spread evenly through the whole tissue so the image still shows the distribution of GABA. It is predominantly localized in the MSDB.

Serotonin was detected at m/z 444.3. The signal intensity was low but the distribution pattern can be visualized very clearly. The serotonin metabolite 5-hydroxyindoleacetic acid (5-HIAA) was detected at m/z 459.3 and it had similar distribution to serotonin but a lower signal-to-noise ratio so that its distribution cannot be seen as clearly as for serotonin.

A signal for the administered compound APO could not be found after search for both the singly and doubly derivatized analog. There were very high signals divided evenly over all the tissues at the m/z values that correspond to the analogs. Also the DA precursor tyrosine and the DA metabolite homovanillic acid could not be visualized because they had strong overlapping signals.

4.4.2 MALDI-MSI with DCHCA

MALDI-MSI was performed with DCHCA for imaging of acetylcholine (ACh) and α-GPC. The results are displayed in Figure 13. ACh was detected at m/z 146.14 and had a signal in the whole tissue but it was strongest in the striatum. There might be a bias in the experiment because the distribution between the right and the left side of the sections were not symmetrical, or rather the right side exhibited a weaker signal for all tissues. At m/z 258.15 α-GPC was detected and was located in the ventral medial part of the brain. The bias observed when looking at ACh did not affect the distribution of α-GPC.

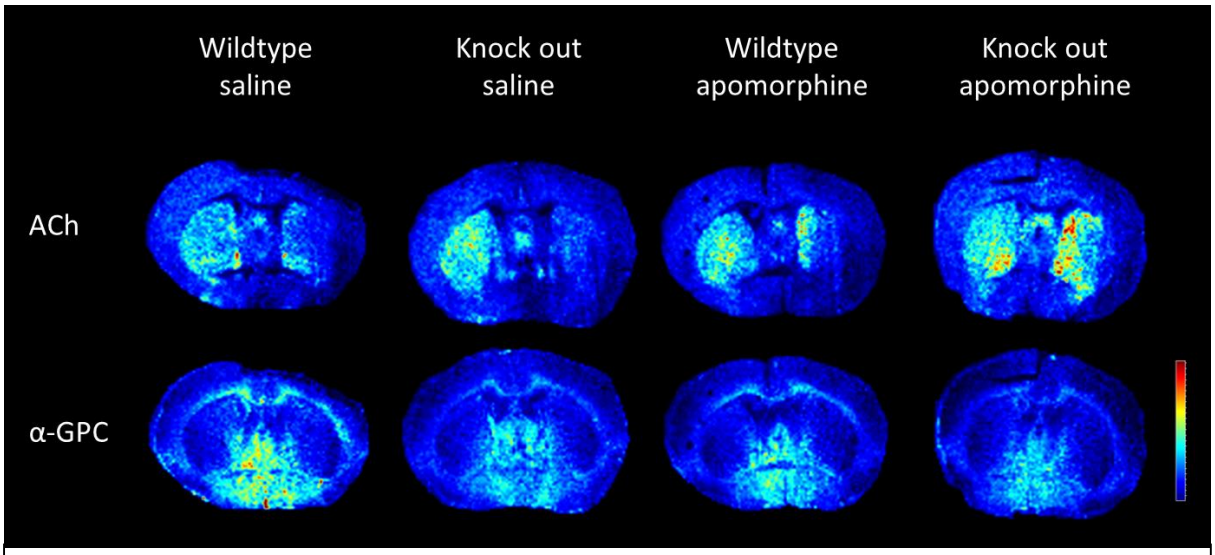

Figure 13. MALDI-MSI of coronal mouse brain tissue sections with DCHCA. One brain section for each group is displayed. Signal intensities are indicated using a rainbow scale. Spatial resolution: 100 µm. The images are TIC normalized.

4.4.3 MALDI-MSI with 9-AA in negative mode

Results from MALDI-MSI in negative mode with 9-AA as matrix are displayed in Figure 14. Glutamate (Glu), glutamine (Gln) and aspartate (Asp) were detected at m/z 146.0, 145.0 and 131.9, respectively. All three compounds were detected in the whole tissue. Glu exhibited lower intensity in the ventral medial part, where the hypothalamus is located and Asp was highest in the cortex and lowest in the striatum.

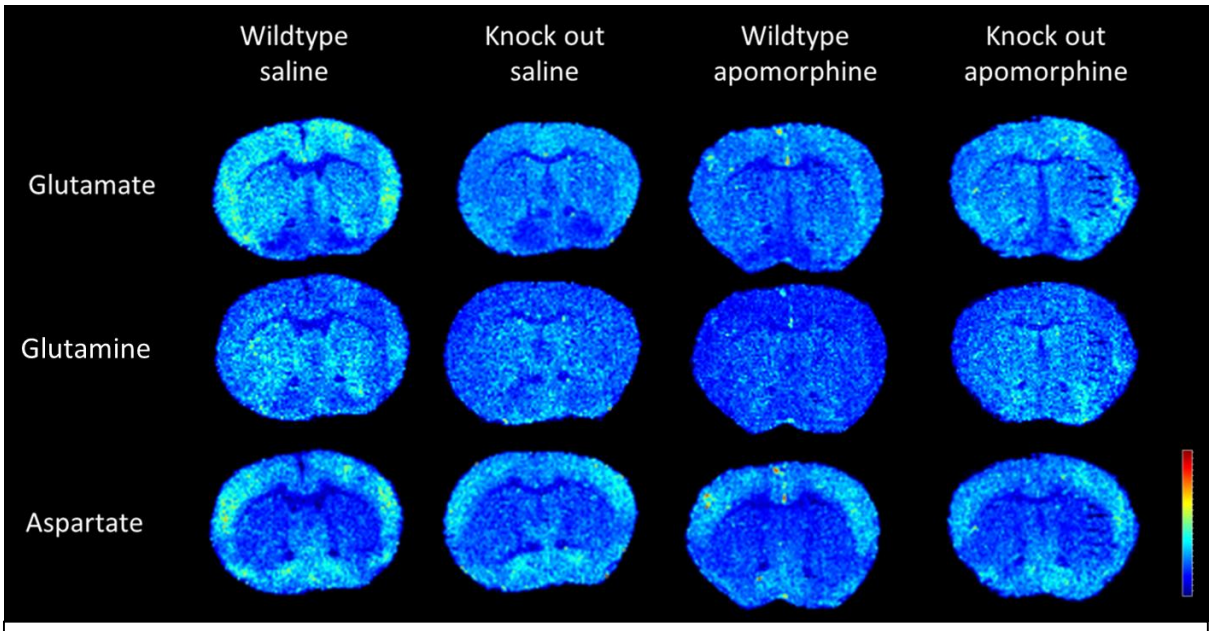

Figure 14. MALDI-MSI of coronal brain tissue sections with 9-AA in negative mode. One brain section for each group is displayed. Signal intensities are indicated using a rainbow scale. Spatial resolution: 100 µm. The images are TIC normalized.

4.5 Pairwise comparison for examining knock-out effect

The imaging of dopamine in the coronal sections revealed that there had been a shortcoming in genotyping. Three of the animals that were supposed to be KO animals had the same DA levels as the WT animals (see Figure B in Appendix II). Therefore, these three animals were excluded from the analysis.

In this pairwise comparison, the WT and KO animals that had received the same treatment were paired. The KO effect was examined by finding the ratio of NTs intensity between WT and KO animals ((NT intensity in WT)/ (NT intensity KO)). Then the averages of the ratios were calculated. There were two pairs in the SAL treated group and three in the APO treated group.

4.5.1 Dopamine

Figure 15 shows the results for dopamine. SAL treated animals showed larger differences than the APO treated. But when looking at only the CP the difference is not as big as in the whole tissue.

4.5.2 Acetylcholine

The MALDI images of acetylcholine (ACh) might have been defected as mentioned before. However, they supported the results from the previous experiment, that ACh is higher in KO than WT (Figure 16).

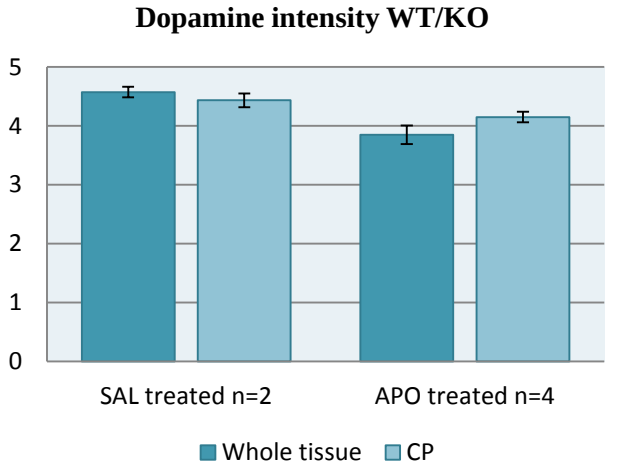

Figure 16. Pairwise comparison to examine treatment effect on DA intensity. The ratios between WT and KO animals for each treatment group are displayed. The standard deviation (SD) is marked on the

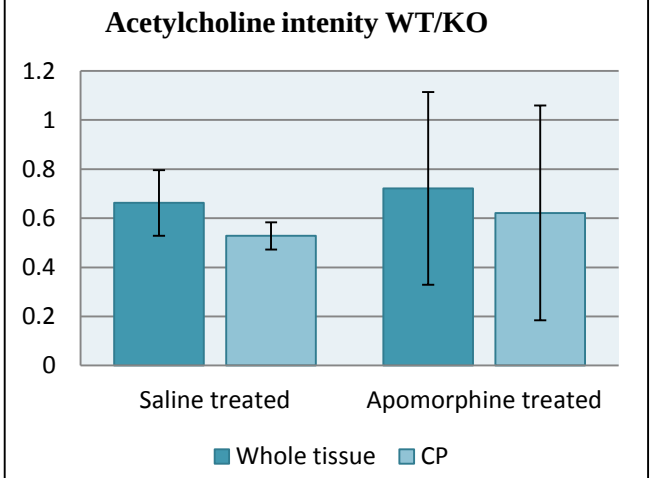

Figure 15. Results from the pairwise comparison for examining KO effect in SAL treated and APO treated mice. ACh levels in WT divided by ACh levels in KO are displayed. The SD is marked on the

4.5.3 Glutamate, glutamine and aspartate

For SAL treated animals the three negatively charged amino acids were higher in WT than in KO but not in APO treated. The increase was about 20% (Figure 17).

GABA and serotonin did not show any notable differences and had a ratio in the range of 1.00 ± 0.10.

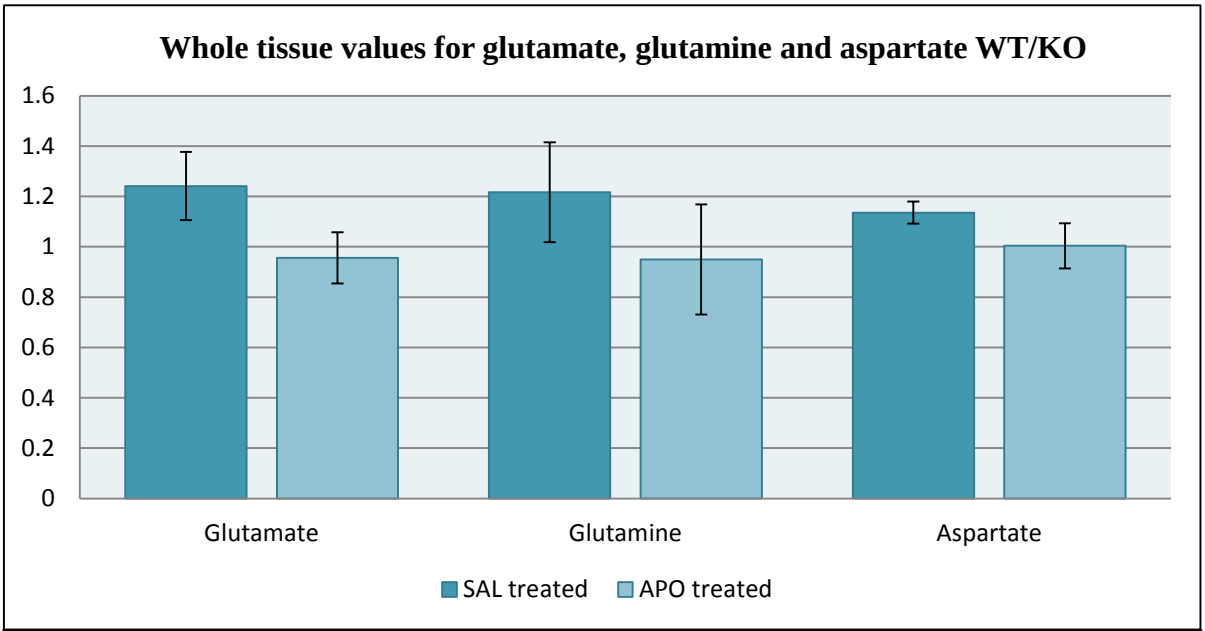

Figure 17. Pairwise comparison to examine KO effect on Glu, Gln and Asp. The ratios between the WT and KO animals for each treatment groups are displayed. The SD is marked on the columns.

4.6 Pairwise comparison for examining treatment effect

When examining treatment effect each apomorphine (APO) treated animal was pared with a saline (SAL) treated animal with the same genotype. The ratios were calculated by dividing values for APO treated animals with values for saline treated animals. There were four pairs in the WT group and two in the KO group.

For KO animals, APO treated subject were about 50% higher in dopamine than saline treated. This effect was not as pronounced for WT treated animals where the difference was around 20%. The result had a large standard deviation (Figure 18). 3-MT was also increased in APO treated animals to about 20%.

For WT animals, APO treatment decreased glutamate, glutamine and aspartate but in KO animals the levels were not affected. The decrease was about 15% for all molecules. The SD were quite low and are displayed in Figure 19.

Other analytes were not affected by APO treatment and had a ratio in the range of 1.00 ± 0.10.

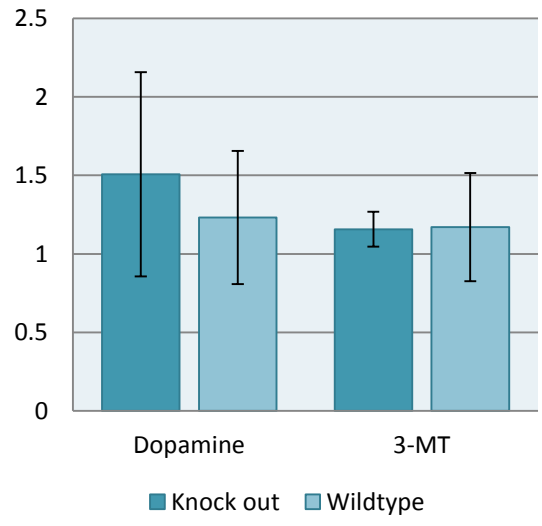

Figure 18. Pairwise comparison to examine treatment effect on DA and 3-MT. The ratios between the APO treated and SAL treated animals for each genotype are displayed. The SD is marked on the columns.

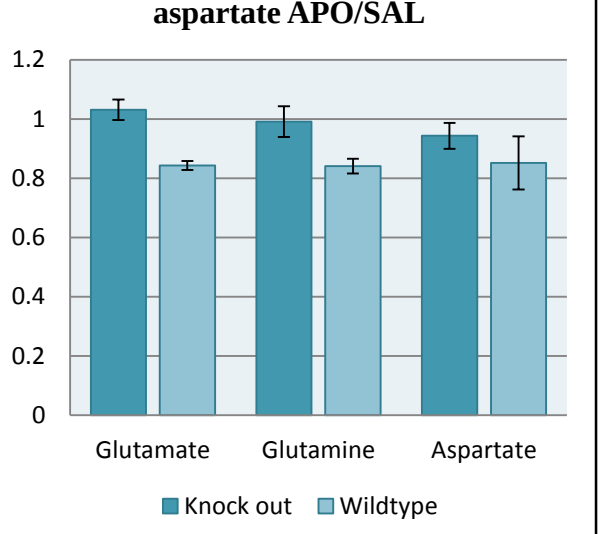

Figure 19. Pairwise comparison to examine treatment effect on Glu, Gln and Asp. The ratios between the APO treated and SAL treated animals for each genotype are displayed. The SD is marked on the columns.

5. DISCUSSION

Knocking out the Nurr1 gene has demonstrated a dopaminergic dysfunction that mimics the progressive stages of Parkinson's (Kadkhodaei et al., 2013). In the present study MALDI-MSI was used in order to examine the effects on neuronal communication by mapping the distribution of neurotransmitters in wild type mice and in Nurr1 knock-out mouse models.

5.1 Decreased dopamine levels in knock-out animals and old wild type animals

A 70% decrease in striatal dopamine (DA) levels in adult animals was measured but in old animals the difference was only around 55%. Results from HPLC measurements in old animals have previously shown that the decrease was more than 80% for old animals (Kadkhodaei, 2013). There may be factors that can explain this variation. The HPLC are measured using extracts of the whole brain structures whereas here only a thin section is measured and DA concentration might differ depending on the level of the brain. The extract would give an average concentration in the whole structure but MALDI-MSI provides quantitative information specific for the certain level of the brain. However the advantages of using MALDI-MSI compared to HPLC is that it allows measuring of concentration in many structure at once and many molecules can be detected in the same measurement.

It is interesting to note the age related decrease in DA between the 4-7 month old group and the 11 month old. In only 6 months the DA decreased about 50% in the vCP and NAc. It is clear that DA levels decrease due to ageing. This adds another variable to the evaluation because the exact age of the animals is not known.

5.2 Acetylcholine increased in Nurr1 knock-out animals

In respect to age, acetylcholine (ACh) had an average increase of 24% for all structures measured in the KO animals in sagittal sections. The coronal experiment suffered from a bias mentioned earlier (section 4.4.2) but the results supported that ACh is increased in KO. The defect might have occurred during cutting or preparing the samples. However, the bias was not seen for α-GPC, neither for other peaks that were checked suggesting that there was a breakdown that only affected ACh but no other molecules of interest.

There is not much in the literature that states that ACh is increased in PD. ACh is a very unstable compound and breaks down quickly which might be the reason for why it has not been measured before in a PD model (Goodwin, 2012). Most research focuses on measuring

nicotinic cholinergic receptors but do not measure ACh directly (Guan, Nordberg, Mousavi, Rinne, & Hellström-Lindahl, 2002; Oishi et al., 2007; Schmaljohann et al., 2006; Schröder et al., 1995). These references suggest a decrease in the nicotinic acetylcholine receptor protein in PD. The imbalance between DA and ACh in PD is frequently mentioned (Calabresi et al., 2006). Due to the decrease in DA levels a relative cholinergic over activity occurs (Spehlmann & Stahl, 1976; Weingarten et al., 2015). Anticholinergic agents have been used to make up for this imbalance even before L-DOPA treatment was discovered (Clarke, 2004). Some ACh synthesizing neurons undergo degeneration in PD (Hirsch, Graybiel, Duyckaerts, & Javoy-Agid, 1987; Perry et al., 1985). However the striatal cholinergic system seems to be spared in PD and it has been suggested that the DAergic nigrostriatal degeneration could result in sprouting of new axons of cholinergic interneurons in the caudate nucleus (Calabresi et al., 2006). The increase in ACh observed in this report support this suggestion. The increase in ACh suggests that the relative cholinergic over activity in PD is not only due to the decreased DA levels but also due to increase in ACh levels. It also might explain why anticholinergic treatment is an effective for symptoms of PD.

5.3 Glutamate, glutamine and aspartate

Glutamate is a common neurotransmitter in the basal ganglia and is considered to be altered towards a glutamateric hyperactivity in PD (Carrillo-Mora, Silva-Adaya, & Villaseñor-Aguayo, 2013). Results from sagittal samples showed a decrease in Glu and aspartate (Asp) both due to knocking out Nurr1 and due to ageing. Glutamine (Gln) however increased gradually in the opposite order to Glu and Asp.

The results from the coronal samples showed a different pattern for Gln where it was decreased in KO animals. The SAL treated group showed about 20% increase in all three molecules in WT animals compared to KO animals. It should be noted that only two pairs were included in the SAL treated group so it is not relevant to draw conclusions from the bars or standard deviation for that group. The APO group should therefore be a better representative for the KO effect but that group did not show any significant difference between KO and WT animals in the three molecules Gln, Glu and Asp.

Considering the inconsistency in the results for the sagittal and coronal experiments it is hard to draw a conclusion on the KO effect on these three amino acids. This research has a lot of variables (different genotypes, different ages and different treatment) and they complicate the

final assumption on if there is any discrepancy in the concentrations of these molecules in the KO model compared to WT.

APO treated WT animals exhibited lower levels of Gln, Glu and Asp than SAL treated suggesting that APO treatment decreases the levels of these molecules. A previous research in a 6-OHDA lesion rodent PD model reported that APO treatment did not affect the concentration of striatal Glu (Touchon et al., 2005). This research used microdialysis to measure the extracellular concentration of Glu in the striatum. Both the type of PD model and the analytical method might explain the difference in the results.

5.4 Apomorphine increased dopamine and 3-MT levels

APO treated animals exhibited higher DA than SAL treated. The increase was greater in the KO animals (about 50%) than in the SAL treated animals (about 23%). The KO group only contained 2 pairs and the SD were quite big so further evaluation on a bigger group of subjects should be done before drawing conclusions. The DA metabolite 3-MT was also increased in APO treated animals about 17%. These results suggest that treatment with the DAergic agonist APO might contribute to symptomatic relief both by activating DA receptors and by increasing levels of DA in the striatum.

5.5 Strengths and limitations

Several things should be kept in mind when evaluating the results. It can be troublesome to cut same depth level of the tissues section for all animals that are being compared. To get the best results they should all be from the same level. In this research it was not a significant problem for the sagittal samples but the coronal samples varied more in depth. As mentioned before, age of the subjects might affect the results because of age related variation on NTs. The number of subjects in each group being compared was low, and varied from n=2 to n=5 so care should be taken when drawing statistical conclusion from the results. Also degradation and delocalization of analytes might take place if sample preparation and tissue handling is not performed carefully. Some brain structures were difficult to see so a staining procedure was applied to ease the optical visualization. The staining helped with the sagittal samples but not with the coronal samples. Another type of staining could have been more useful that targets proteins that are located in specific regions for example acetylcholine esterase for ACh specific regions or TH to see the DA specific regions. Dividing the tissue into regions using ROIs did not show any notable region specific discrepancies apart from for DA and 3-MT in the striatum.

Despite these complications mentioned above, the enormous amount of information that was gathered in this research proves what a powerful tool MALDI-MSI is. Ten different molecules of interest were analyzed following only three different preparation protocols. The distributions of these molecules were mapped and structure specific data was generated. Applying MALDI-MSI to the Nurr1 KO PD model provided new information about ACh that had not been recorded before, but was in correlation to previous studies.

6. CONCLUSIONS

The present study provides new insight into changes in neuronal communication in Parkinson's disease by utilizing MALDI-MSI. It suggests that not only dopamine is effected in PD but other neurotransmitters as well. Acetylcholine seems to be increased and glutamate, glutamine and aspartate might be altered as well. These changes could contribute to both motor and non-motor symptoms of the disease. The study also suggests that dopaminergic treatment with apomorphine increases dopamine levels in the striatum both in PD and in healthy subjects.

In PD research the search for a neuroprotective agent is ongoing. Studies on neurotransmission provide valuable information about the nature of the disease which could lead to a better understanding of its pathogenesis.

The progressive Nurr1 knock-out model allows research on the early stages of the disease. That is important when searching for biomarkers and neuroprotective treatment. Additional analysis of the model might further explain the contribution of Nurr1 to PD and it could be used as an experimental model when trying effectiveness of new therapeutical agents.

7. ACKNOWLEDGEMENTS

The work presented in this thesis was carried out in the research facilities of the Biomolecular Imaging and Proteomics unit in Uppsala University. I am very grateful for getting this opportunity to work in such an advanced research environment.

I want to thank Margrét Þorsteinsdóttir for getting me in touch with the research team in Uppsala and for her guidance in this project. I want to thank my instructors Per Andrén, Mohammadreza Shariatgorji and Anna Nilson for giving me advice and help when needed. You have been an integral part in the development of my research abilities.

I would also like to thank Patrik Källback for helping me out with the software, Lena Norgren for assisting with histological staining and Theodosia Vallianato for always being ready to advice and support me throughout the entire project. I greatly appreciate your help.

Finally, I want to thank my parents and family who have supported me through my education. Your support has been invaluable.

8. REFERENCES

Allen Institute for Brain Science. (2015). Allen Human Brain Atlas [Internet].

Bäckman, C., Perlmann, T., Wallén, Å., Hoffer, B. J., & Morales, M. (1999). A selective group of dopaminergic neurons express Nurr1 in the adult mouse brain. *Brain Research*, *851*(1–2), 125–132. http://doi.org/10.1016/S0006-8993(99)02149-6

Balluff, B., Schöne, C., Höfler, H., & Walch, A. (2011). MALDI imaging mass spectrometry for direct tissue analysis: technological advancements and recent applications. *Histochemistry and Cell Biology*, *136*(3), 227–244. http://doi.org/10.1007/s00418-011-0843-x

Bastide, M. F., Meissner, W. G., Picconi, B., Fasano, S., Fernagut, P.-O., Feyder, M., … Bézard, E. (2015). Pathophysiology of L-dopa-induced motor and non-motor complications in Parkinson's disease. *Progress in Neurobiology*, *132*, 96–168. http://doi.org/10.1016/j.pneurobio.2015.07.002

Benatru, I., Vaugoyeau, M., & Azulay, J.-P. (2008). Postural disorders in Parkinson's disease. *Neurophysiologie Clinique/Clinical Neurophysiology*, *38*(6), 459–465. http://doi.org/10.1016/j.neucli.2008.07.006

Benson, C., Mifflin, K., Kerr, B., Jesudasan, S. J. B., Dursun, S., & Baker, G. (2015). Biogenic Amines and the Amino Acids GABA and Glutamate: Relationships with Pain and Depression. *Modern Trends in Pharmacopsychiatry*, *30*, 67–79. http://doi.org/10.1159/000435933

Berardelli, A., Sabra, A. F., & Hallett, M. (1983). Physiological mechanisms of rigidity in Parkinson's disease. *Journal of Neurology, Neurosurgery & Psychiatry*, *46*(1), 45–53. http://doi.org/10.1136/jnnp.46.1.45

Blandini, F., Nappi, G., Tassorelli, C., & Martignoni, E. (2000). Functional changes of the basal ganglia circuitry in Parkinson's disease. *Progress in Neurobiology*, *62*(1), 63–88. http://doi.org/10.1016/S0301-0082(99)00067-2

Blaudin de Thé, F.-X., Rekaik, H., Prochiantz, A., Fuchs, J., & Joshi, R. L. (2015). Neuroprotective Transcription Factors in Animal Models of Parkinson Disease. *Neural Plasticity*. Retrieved from http://www.hindawi.com/journals/np/2015/815492/abs/

Bomasang-Layno, E., Fadlon, I., Murray, A. N., & Himelhoch, S. (2015). Antidepressive treatments for Parkinson's disease: A systematic review and meta-analysis.

Parkinsonism & Related Disorders, *21*(8), 833–842. http://doi.org/10.1016/j.parkreldis.2015.04.018

Bonuccelli, U., Del Dotto, P., & Rascol, O. (2009). Role of dopamine receptor agonists in the treatment of early Parkinson's disease. *Parkinsonism & Related Disorders*, *15 Suppl 4*, S44–53. http://doi.org/10.1016/S1353-8020(09)70835-1

Breydo, L., Wu, J. W., & Uversky, V. N. (2012). α-Synuclein misfolding and Parkinson's disease. *Biochimica et Biophysica Acta (BBA) - Molecular Basis of Disease*, *1822*(2), 261–285. http://doi.org/10.1016/j.bbadis.2011.10.002

Brown, P., & Marsden, C. (1998). What do the basal ganglia do? *The Lancet*, *351*(9118), 1801–1804. http://doi.org/10.1016/S0140-6736(97)11225-9

Calabresi, P., Picconi, B., Parnetti, L., & Di Filippo, M. (2006). A convergent model for cognitive dysfunctions in Parkinson's disease: the critical dopamine–acetylcholine synaptic balance. *The Lancet Neurology*, *5*(11), 974–983. http://doi.org/10.1016/S1474-4422(06)70600-7

Cameron, L. C. (2012). Mass spectrometry imaging: Facts and perspectives from a non-mass spectrometrist point of view. *Methods*, *57*(4), 417–422. http://doi.org/10.1016/j.ymeth.2012.06.007

Cantor, R. S. (2015). The evolutionary origin of the need to sleep: an inevitable consequence of synaptic neurotransmission? *Frontiers in Synaptic Neuroscience*, *7*, 15. http://doi.org/10.3389/fnsyn.2015.00015

Caprioli, R. M., Farmer, T. B., & Gile, J. (1997). Molecular Imaging of Biological Samples: Localization of Peptides and Proteins Using MALDI-TOF MS. *Analytical Chemistry*, *69*(23), 4751–4760. http://doi.org/10.1021/ac970888i

Cardoso, S. M. (2011). The mitochondrial cascade hypothesis for Parkinson's disease. *Current Pharmaceutical Design*, *17*(31), 3390–3397.

Carrillo-Mora, P., Silva-Adaya, D., & Villaseñor-Aguayo, K. (2013). Glutamate in Parkinson's disease: Role of antiglutamatergic drugs. *Basal Ganglia*, *3*(3), 147–157. http://doi.org/10.1016/j.baga.2013.09.001

Chaudhuri, K. R., Healy, D. G., & Schapira, A. H. (2006). Non-motor symptoms of Parkinson's disease: diagnosis and management. *The Lancet Neurology*, *5*(3), 235–245. http://doi.org/10.1016/S1474-4422(06)70373-8

Chaudhuri, K. R., & Schapira, A. H. (2009). Non-motor symptoms of Parkinson's disease: dopaminergic pathophysiology and treatment. *The Lancet Neurology*, *8*(5), 464–474. http://doi.org/10.1016/S1474-4422(09)70068-7

Chaurand, P., Schwartz, S. A., Billheimer, D., Xu, B. J., Crecelius, A., & Caprioli, R. M. (2004). Integrating Histology and Imaging Mass Spectrometry. *Analytical Chemistry*, *76*(4), 1145–1155. http://doi.org/10.1021/ac0351264

Chu, Y., Le, W., Kompoliti, K., Jankovic, J., Mufson, E. J., & Kordower, J. H. (2006). Nurr1 in Parkinson's disease and related disorders. *The Journal of Comparative Neurology*, *494*(3), 495–514. http://doi.org/10.1002/cne.20828

Clarke, C. E. (2004). Neuroprotection and pharmacotherapy for motor symptoms in Parkinson's disease. *The Lancet Neurology*, *3*(8), 466–474. http://doi.org/10.1016/S1474-4422(04)00823-3

Dawson, T. M., Ko, H. S., & Dawson, V. L. (2010). Genetic Animal Models of Parkinson's Disease. *Neuron*, *66*(5), 646–661. http://doi.org/10.1016/j.neuron.2010.04.034

Decressac, M., Kadkhodaei, B., Mattsson, B., Laguna, A., Perlmann, T., & Björklund, A. (2012). α-Synuclein–Induced Down-Regulation of Nurr1 Disrupts GDNF Signaling in Nigral Dopamine Neurons. *Science Translational Medicine*, *4*(163), 163ra156–163ra156. http://doi.org/10.1126/scitranslmed.3004676

Decressac, M., Volakakis, N., Björklund, A., & Perlmann, T. (2013). NURR1 in Parkinson disease—from pathogenesis to therapeutic potential. *Nature Reviews Neurology*, *9*(11), 629–636. http://doi.org/10.1038/nrneurol.2013.209

de Lau, L. M., & Breteler, M. M. (2006). Epidemiology of Parkinson's disease. *The Lancet Neurology*, *5*(6), 525–535. http://doi.org/10.1016/S1474-4422(06)70471-9

Delgado, M., & Ganea, D. (2003). Neuroprotective effect of vasoactive intestinal peptide (VIP) in a mouse model of Parkinson's disease by blocking microglial activation. *FASEB Journal: Official Publication of the Federation of American Societies for Experimental Biology*, *17*(8), 944–946. http://doi.org/10.1096/fj.02-0799fje

Deutskens, F., Yang, J., & Caprioli, R. M. (2011). High spatial resolution imaging mass spectrometry and classical histology on a single tissue section. *Journal of Mass Spectrometry*, *46*(6), 568–571. http://doi.org/10.1002/jms.1926

Duty, S., & Jenner, P. (2011). Animal models of Parkinson's disease: a source of novel treatments and clues to the cause of the disease. *British Journal of Pharmacology*, *164*(4), 1357–1391. http://doi.org/10.1111/j.1476-5381.2011.01426.x

Ehringer, H., & Hornykiewicz, O. (1960). Verteilung Von Noradrenalin Und Dopamin (3-Hydroxytyramin) Im Gehirn Des Menschen Und Ihr Verhalten Bei Erkrankungen Des Extrapyramidalen Systems. *Klinische Wochenschrift*, *38*(24), 1236–1239. http://doi.org/10.1007/BF01485901

Engblom, D., Bilbao, A., Sanchis-Segura, C., Dahan, L., Perreau-Lenz, S., Balland, B., … Spanagel, R. (2008). Glutamate Receptors on Dopamine Neurons Control the Persistence of Cocaine Seeking. *Neuron*, *59*(3), 497–508. http://doi.org/10.1016/j.neuron.2008.07.010

Eriksson, C., Masaki, N., Yao, I., Hayasaka, T., & Setou, M. (2013). MALDI Imaging Mass Spectrometry—A Mini Review of Methods and Recent Developments. *Mass Spectrometry*, *2*(Spec Iss). http://doi.org/10.5702/massspectrometry.S0022

Eskow Jaunarajs, K. L., Angoa-Perez, M., Kuhn, D. M., & Bishop, C. (2011). Potential mechanisms underlying anxiety and depression in Parkinson's disease: consequences of l-DOPA treatment. *Neuroscience and Biobehavioral Reviews*, *35*(3), 556–564. http://doi.org/10.1016/j.neubiorev.2010.06.007

Fuke, S., Kubota-Sakashita, M., Kasahara, T., Shigeyoshi, Y., & Kato, T. (2011). Regional variation in mitochondrial DNA copy number in mouse brain. *Biochimica et Biophysica Acta (BBA) - Bioenergetics*, *1807*(3), 270–274. http://doi.org/10.1016/j.bbabio.2010.11.016

Galleguillos, D., Fuentealba, J. A., Gómez, L. M., Saver, M., Gómez, A., Nash, K., … Andrés, M. E. (2010). Nurr1 regulates RET expression in dopamine neurons of adult rat midbrain. *Journal of Neurochemistry*, *114*(4), 1158–1167. http://doi.org/10.1111/j.1471-4159.2010.06841.x

Gasser, T. (2001). Genetics of Parkinson's disease. *Journal of Neurology*, *248*(10), 833–840. http://doi.org/10.1007/s004150170066

Gautier, C. A., Corti, O., & Brice, A. (2014). Mitochondrial dysfunctions in Parkinson's disease. *Revue Neurologique*, *170*(5), 339–343. http://doi.org/10.1016/j.neurol.2013.06.003

Goedert, M., Spillantini, M. G., Del Tredici, K., & Braak, H. (2013). 100 years of Lewy pathology. *Nature Reviews. Neurology*, *9*(1), 13–24. http://doi.org/10.1038/nrneurol.2012.242

Goodwin, R. J. A. (2012). Sample preparation for mass spectrometry imaging: Small mistakes can lead to big consequences. *Journal of Proteomics*, *75*(16), 4893–4911. http://doi.org/10.1016/j.jprot.2012.04.012

Grimes, D. A., Han, F., Panisset, M., Racacho, L., Xiao, F., Zou, R., … Bulman, D. E. (2006). Translated mutation in the Nurr1 gene as a cause for Parkinson's disease. *Movement Disorders: Official Journal of the Movement Disorder Society*, *21*(7), 906–909. http://doi.org/10.1002/mds.20820

Guan, Z.-Z., Nordberg, A., Mousavi, M., Rinne, J. O., & Hellström-Lindahl, E. (2002). Selective changes in the levels of nicotinic acetylcholine receptor protein and of corresponding mRNA species in the brains of patients with Parkinson's disease. *Brain Research*, *956*(2), 358–366. http://doi.org/10.1016/S0006-8993(02)03571-0

Gubellini, P., & Kachidian, P. (2015). Animal models of Parkinson's disease: An updated overview. *Revue Neurologique*. http://doi.org/10.1016/j.neurol.2015.07.011

Hardy, J., Lewis, P., Revesz, T., Lees, A., & Paisan-Ruiz, C. (2009). The genetics of Parkinson's syndromes: a critical review. *Current Opinion in Genetics & Development*, *19*(3), 254–265. http://doi.org/10.1016/j.gde.2009.03.008

Hartl, F. U., Bracher, A., & Hayer-Hartl, M. (2011). Molecular chaperones in protein folding and proteostasis. *Nature*, *475*(7356), 324–332. http://doi.org/10.1038/nature10317

Hegarty, S. V., Sullivan, A. M., & O'Keeffe, G. W. (2013). Midbrain dopaminergic neurons: A review of the molecular circuitry that regulates their development. *Developmental Biology*, *379*(2), 123–138. http://doi.org/10.1016/j.ydbio.2013.04.014

Hirsch, E. C., Graybiel, A. M., Duyckaerts, C., & Javoy-Agid, F. (1987). Neuronal loss in the pedunculopontine tegmental nucleus in Parkinson disease and in progressive supranuclear palsy. *Proceedings of the National Academy of Sciences of the United States of America*, *84*(16), 5976–5980.

Hisahara, S., Shimohama, S., Hisahara, S., & Shimohama, S. (2011). Dopamine Receptors and Parkinson's Disease, Dopamine Receptors and Parkinson's Disease. *International Journal of Medicinal Chemistry*, *International Journal of Medicinal Chemistry*, *2011*, *2011*, e403039. http://doi.org/10.1155/2011/403039, 10.1155/2011/403039

Jankovic, J. (2008). Parkinson's disease: clinical features and diagnosis. *Journal of Neurology, Neurosurgery & Psychiatry*, *79*(4), 368–376. http://doi.org/10.1136/jnnp.2007.131045

Jankovic, J., Chen, S., & Le, W. D. (2005). The role of Nurr1 in the development of dopaminergic neurons and Parkinson's disease. *Progress in Neurobiology*, *77*(1–2), 128–138. http://doi.org/10.1016/j.pneurobio.2005.09.001

Jiang, C., Wan, X., He, Y., Pan, T., Jankovic, J., & Le, W. (2005). Age-dependent dopaminergic dysfunction in Nurr1 knockout mice. *Experimental Neurology*, *191*(1), 154–162. http://doi.org/10.1016/j.expneurol.2004.08.035

Kadkhodaei, B., Alvarsson, A., Schintu, N., Ramsköld, D., Volakakis, N., Joodmardi, E., … Perlmann, T. (2013). Transcription factor Nurr1 maintains fiber integrity and nuclear-

encoded mitochondrial gene expression in dopamine neurons. *Proceedings of the National Academy of Sciences*, *110*(6), 2360–2365. http://doi.org/10.1073/pnas.1221077110

Kadkhodaei, B., Ito, T., Joodmardi, E., Mattsson, B., Rouillard, C., Carta, M., … Perlmann, T. (2009). Nurr1 Is Required for Maintenance of Maturing and Adult Midbrain Dopamine Neurons. *The Journal of Neuroscience*, *29*(50), 15923–15932. http://doi.org/10.1523/JNEUROSCI.3910-09.2009

Kakkar, A. K., & Dahiya, N. (2015). Management of Parkinson′s disease: Current and future pharmacotherapy. *European Journal of Pharmacology*, *750*, 74–81. http://doi.org/10.1016/j.ejphar.2015.01.030

Karas, M., & Hillenkamp, F. (1988). Laser desorption ionization of proteins with molecular masses exceeding 10,000 daltons. *Analytical Chemistry*, *60*(20), 2299–2301.

Lees, A. J., Hardy, J., & Revesz, T. (2009). Parkinson's disease. *The Lancet*, *373*(9680), 2055–2066. http://doi.org/10.1016/S0140-6736(09)60492-X

Le, W., Pan, T., Huang, M., Xu, P., Xie, W., Zhu, W., … Jankovic, J. (2008). Decreased NURR1 gene expression in patients with Parkinson's disease. *Journal of the Neurological Sciences*, *273*(1-2), 29–33. http://doi.org/10.1016/j.jns.2008.06.007

Le, W., Xu, P., Jankovic, J., Jiang, H., Appel, S. H., Smith, R. G., & Vassilatis, D. K. (2003). Mutations in NR4A2 associated with familial Parkinson disease. *Nature Genetics*, *33*(1), 85–89. http://doi.org/10.1038/ng1066

Li, L., Su, Y., Zhao, C., Zhao, H., Liu, G., Wang, J., & Xu, Q. (2006). The role of Ret receptor tyrosine kinase in dopaminergic neuron development. *Neuroscience*, *142*(2), 391–400. http://doi.org/10.1016/j.neuroscience.2006.06.018

Lin, M. T., & Beal, M. F. (2006). Mitochondrial dysfunction and oxidative stress in neurodegenerative diseases. *Nature*, *443*(7113), 787–795. http://doi.org/10.1038/nature05292

Luo, Y. (2012). The function and mechanisms of Nurr1 action in midbrain dopaminergic neurons, from development and maintenance to survival. *International Review of Neurobiology*, *102*, 1–22. http://doi.org/10.1016/B978-0-12-386986-9.00001-6

Maxwell, S. L., Ho, H.-Y., Kuehner, E., Zhao, S., & Li, M. (2005). Pitx3 regulates tyrosine hydroxylase expression in the substantia nigra and identifies a subgroup of mesencephalic dopaminergic progenitor neurons during mouse development. *Developmental Biology*, *282*(2), 467–479. http://doi.org/10.1016/j.ydbio.2005.03.028

Meding, S., & Walch, A. (2013). MALDI imaging mass spectrometry for direct tissue analysis. *Methods in Molecular Biology (Clifton, N.J.)*, *931*, 537–546. http://doi.org/10.1007/978-1-62703-056-4_29

Michell, A. W., Lewis, S. J. G., Foltynie, T., & Barker, R. A. (2004). Biomarkers and Parkinson's disease. *Brain*, *127*(8), 1693–1705. http://doi.org/10.1093/brain/awh198

Mollenhauer, B., & Zhang, J. (2012). Biochemical premotor biomarkers for Parkinson's disease. *Movement Disorders*, *27*(5), 644–650. http://doi.org/10.1002/mds.24956

Müller, T. (2012). Drug therapy in patients with Parkinson's disease. *Translational Neurodegeneration*, *1*(1), 10. http://doi.org/10.1186/2047-9158-1-10

Norris, J. L., & Caprioli, R. M. (2013). Analysis of Tissue Specimens by Matrix-Assisted Laser Desorption/Ionization Imaging Mass Spectrometry in Biological and Clinical Research. *Chemical Reviews*, *113*(4), 2309–2342. http://doi.org/10.1021/cr3004295

Oishi, N., Hashikawa, K., Yoshida, H., Ishizu, K., Ueda, M., Kawashima, H., … Fukuyama, H. (2007). Quantification of nicotinic acetylcholine receptors in Parkinson's disease with 123I-5IA SPECT. *Journal of the Neurological Sciences*, *256*(1–2), 52–60. http://doi.org/10.1016/j.jns.2007.02.014

Perry, E. K., Curtis, M., Dick, D. J., Candy, J. M., Atack, J. R., Bloxham, C. A., … Tomlinson, B. E. (1985). Cholinergic correlates of cognitive impairment in Parkinson's disease: Comparisons with Alzheimer's disease. *Journal of Neurology Neurosurgery and Psychiatry*, *48*(5), 413–421.

Pfeiffer, R. F. (2015). Non-motor symptoms in Parkinson's disease. *Parkinsonism & Related Disorders*. http://doi.org/10.1016/j.parkreldis.2015.09.004

Rizzo, G., Arcuti, S., Martino, D., Copetti, M., Fontana, A., & Logroscino, G. (2015). Accuracy of Clinical Diagnosis of Parkinson's Disease: A Systematic Review and Bayesian Meta-Analysis (S36.001). *Neurology*, *84*(14 Supplement), S36.001.

Römpp, A., & Spengler, B. (2013). Mass spectrometry imaging with high resolution in mass and space. *Histochemistry and Cell Biology*, *139*(6), 759–783. http://doi.org/10.1007/s00418-013-1097-6

Santos, D., & Cardoso, S. M. (2012). Mitochondrial dynamics and neuronal fate in Parkinson's disease. *Mitochondrion*, *12*(4), 428–437. http://doi.org/10.1016/j.mito.2012.05.002

Schapira, A. H. V. (2008). Progress in neuroprotection in Parkinson's disease. *European Journal of Neurology*, *15*, 5–13. http://doi.org/10.1111/j.1468-1331.2008.02055.x

Schmaljohann, J., Gündisch, D., Minnerop, M., Bucerius, J., Joe, A., Reinhardt, M., … Wüllner, U. (2006). In vitro evaluation of nicotinic acetylcholine receptors with 2-[18F]F-A85380 in Parkinson's disease. *Nuclear Medicine and Biology*, *33*(3), 305–309. http://doi.org/10.1016/j.nucmedbio.2005.12.012

Schröder, H., de Vos, R. A. I., Jansen, E. N. H., Birtsch, C., Wevers, A., Lobron, C., … Maelicke, A. (1995). Gene expression of the nicotinic acetylcholine receptor α4 subunit in the frontal cortex in Parkinson's disease patients. *Neuroscience Letters*, *187*(3), 173–176. http://doi.org/10.1016/0304-3940(95)11367-6

Segovia, G., Porras, A., Del Arco, A., & Mora, F. (2001). Glutamatergic neurotransmission in aging: a critical perspective. *Mechanisms of Ageing and Development*, *122*(1), 1–29. http://doi.org/10.1016/S0047-6374(00)00225-6

Shariatgorji, M., Nilsson, A., Goodwin, R. J. A., Källback, P., Schintu, N., Zhang, X., … Andren, P. E. (2014). Direct Targeted Quantitative Molecular Imaging of Neurotransmitters in Brain Tissue Sections. *Neuron*, *84*(4), 697–707. http://doi.org/10.1016/j.neuron.2014.10.011

Shariatgorji, M., Nilsson, A., Goodwin, R. J. A., Svenningsson, P., Schintu, N., Banka, Z., … Andren, P. E. (2012). Deuterated Matrix-Assisted Laser Desorption Ionization Matrix Uncovers Masked Mass Spectrometry Imaging Signals of Small Molecules. *Analytical Chemistry*, *84*(16), 7152–7157. http://doi.org/10.1021/ac301498m

Sharma, S., Singh, S., Sharma, V., Singh, V. P., & Deshmukh, R. (2015). Neurobiology of l-DOPA induced dyskinesia and the novel therapeutic strategies. *Biomedicine & Pharmacotherapy*, *70*, 283–293. http://doi.org/10.1016/j.biopha.2015.01.029

Shetty, A. K., & Bates, A. (2015). Potential of GABA-ergic cell therapy for schizophrenia, neuropathic pain, and Alzheimer′s and Parkinson′s diseases. *Brain Research*. http://doi.org/10.1016/j.brainres.2015.09.019

Simon, H. H., Bhatt, L., Gherbassi, D., Sgadó, P., & Alberí, L. (2003). Midbrain Dopaminergic Neurons. *Annals of the New York Academy of Sciences*, *991*(1), 36–47. http://doi.org/10.1111/j.1749-6632.2003.tb07461.x

Smidt, M. P., & Burbach, J. P. H. (2007). How to make a mesodiencephalic dopaminergic neuron. *Nature Reviews Neuroscience*, *8*(1), 21–32. http://doi.org/10.1038/nrn2039

Spehlmann, R., & Stahl, S. (1976). DOPAMINE ACETYLCHOLINE IMBALANCE IN PARKINSON'S DISEASE: Possible Regenerative Overgrowth of Cholinergic Axon Terminals. *The Lancet*, *307*(7962), 724–726. http://doi.org/10.1016/S0140-6736(76)93095-6

Sugiura, Y., Zaima, N., Setou, M., Ito, S., & Yao, I. (2012). Visualization of acetylcholine distribution in central nervous system tissue sections by tandem imaging mass spectrometry. *Analytical and Bioanalytical Chemistry*, *403*(7), 1851–1861. http://doi.org/10.1007/s00216-012-5988-5

Terzioglu, M., & Galter, D. (2008). Parkinson's disease: genetic versus toxin-induced rodent models. *FEBS Journal*, *275*(7), 1384–1391. http://doi.org/10.1111/j.1742-4658.2008.06302.x

Touchon, J. C., Holmer, H. K., Moore, C., McKee, B. L., Frederickson, J., & Meshul, C. K. (2005). Apomorphine-induced alterations in striatal and substantia nigra pars reticulata glutamate following unilateral loss of striatal dopamine. *Experimental Neurology*, *193*(1), 131–140. http://doi.org/10.1016/j.expneurol.2004.11.023

Wakabayashi, K., Tanji, K., Mori, F., & Takahashi, H. (2007). The Lewy body in Parkinson's disease: Molecules implicated in the formation and degradation of α-synuclein aggregates. *Neuropathology*, *27*(5), 494–506. http://doi.org/10.1111/j.1440-1789.2007.00803.x

Walch, A., Rauser, S., Deininger, S.-O., & Höfler, H. (2008). MALDI imaging mass spectrometry for direct tissue analysis: a new frontier for molecular histology. *Histochemistry and Cell Biology*, *130*(3), 421–434. http://doi.org/10.1007/s00418-008-0469-9

Weingarten, C. P., Sundman, M. H., Hickey, P., & Chen, N.-K. (2015). Neuroimaging of Parkinson's disease: Expanding views. *Neuroscience and Biobehavioral Reviews*. http://doi.org/10.1016/j.neubiorev.2015.09.007

Ye, H., Wang, J., Greer, T., Strupat, K., & Li, L. (2013). Visualizing neurotransmitters and metabolites in the central nervous system by high resolution and high accuracy mass spectrometric imaging. *ACS Chemical Neuroscience*, *4*(7), 1049–1056. http://doi.org/10.1021/cn400065k

Zetterström, R. H., Solomin, L., Jansson, L., Hoffer, B. J., Olson, L., & Perlmann, T. (1997). Dopamine Neuron Agenesis in Nurr1-Deficient Mice. *Science*, *276*(5310), 248–250. http://doi.org/10.1126/science.276.5310.248

Zheng, K., Heydari, B., & Simon, D. K. (2003). A common NURR1 polymorphism associated with Parkinson disease and diffuse Lewy body disease. *Archives of Neurology*, *60*(5), 722–725. http://doi.org/10.1001/archneur.60.5.722

9. APPENDIX

Appendix I: Results from hematoxylin and eosin staining of sagittal tissues

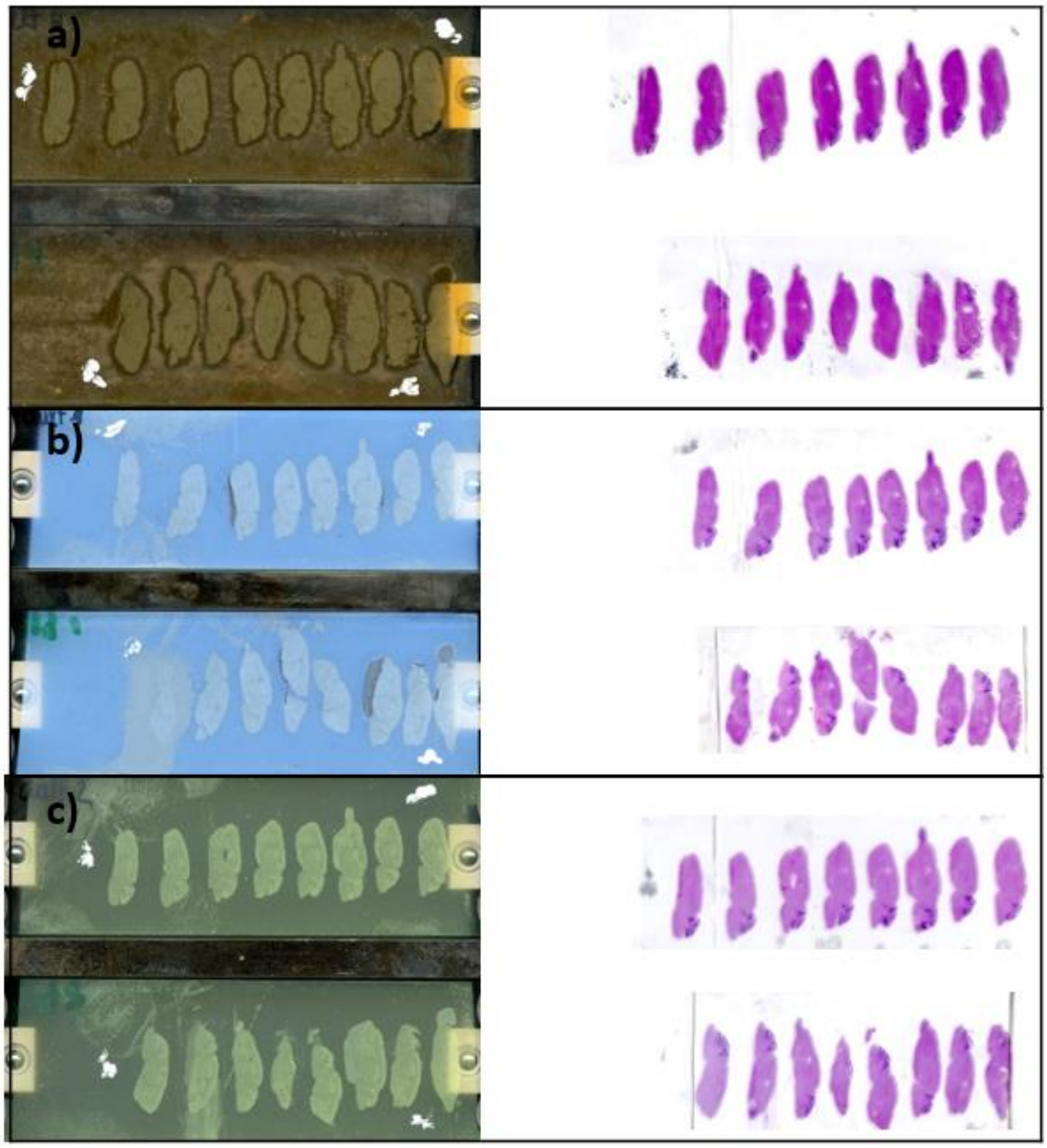

Figure A. Images prior to H&E staining are displayed on the left and the same tissue sections after H&E staining on the right. a) DPP derivatized brain tissue sections. b) Brain tissue sections with DCHCA matrix. c) Brain tissue sections with 9-AA matrix

Appendix II: MALDI-MSI of dopamine in coronal brain tissue sections

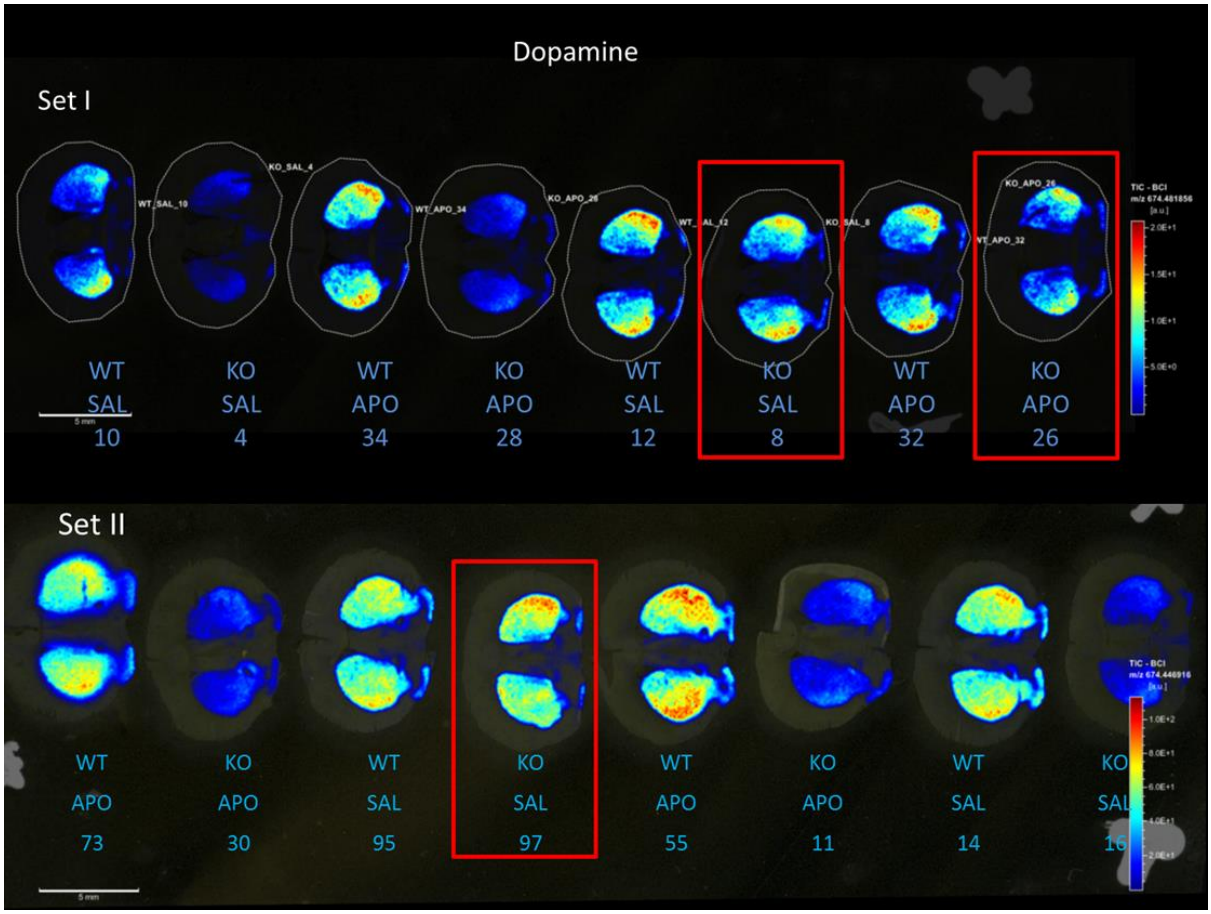

Figure B: Images of DA in coronal brain tissue sections. Below each brain tissue section the expected genotypes, treatment type and number of the animal are indicated. Animals number 8, 26 and 97 exhibited abnormally high DA for KO animals and were excluded from the quantitation analysis.

Appendix III: Chemical structures of molecules measured with MALDI-MSI

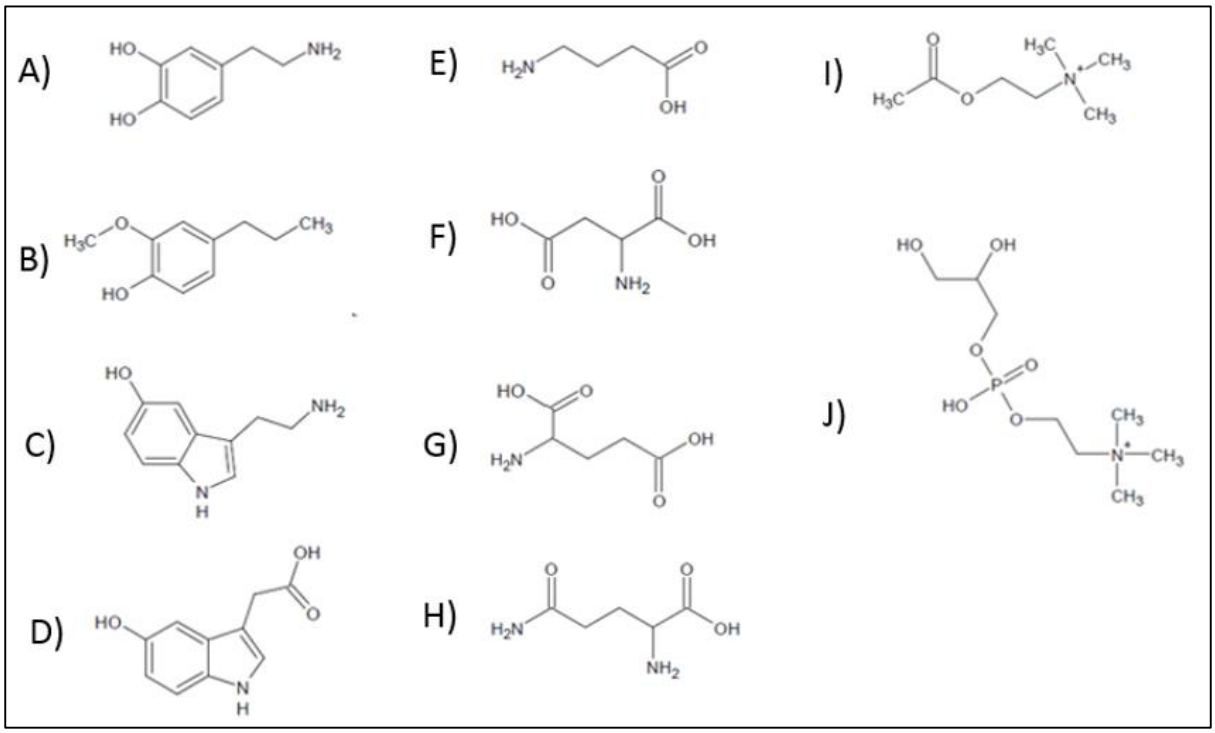

Figure C. Chemical structures of the target molecules that were measured with MALDI-MSI. A) dopamine, B) 3-MT C) serotonin, D) 5-HIAA, E) GABA, F) aspartate, G) glutamate, H) glutamine, I) acetylcholine, J) α-GCP.